RadioGraphics

Classic Signs in Uroradiology[1]

Raymond B. Dyer, MD • Michael Y. Chen, MD • Ronald J. Zagoria, MD

CME FEATURE

See accompanying test at http://www.rsna.org/education/rg_cme.html

LEARNING OBJECTIVES FOR TEST 6

After reading this article and taking the test, the reader will be able to:

- Recognize radiologic signs associated with urinary tract disease.
- Describe the pathophysiologic characteristics associated with the radiologic findings.
- Apply the illustrated signs across imaging modalities.

The language of radiology is rich with descriptions of imaging findings, often metaphorical, which have found common usage in the day-to-day practice of genitourinary radiology. These "classic signs" give us confidence in our diagnosis. Some of the signs have become so familiar to us that they are referred to as an "Aunt Minnie." When the sign is invoked, or an Aunt Minnie is recognized, it often brings an impression of the image to mind, and it may have specific diagnostic and pathologic implications. The article uses classic signs accumulated from the literature to review a variety of pathologic conditions in the urinary tract.

Index terms: Genitourinary system, CT, 80.1211 • Genitourinary system, MR, 80.12141 • Genitourinary system, radiography, 80.122, 80.123 Genitourinary system, US, 80.1298

RadioGraphics 2004; 24:S247–S280 • **Published online** 10.1148/rg.24si045509 • **Content Code:** GU

[1]From the Department of Radiology, Wake Forest University School of Medicine, Medical Center Blvd, Winston-Salem, NC 27157. Recipient of a Certificate of Merit award for an education exhibit at the 2003 RSNA scientific assembly. Received February 17, 2004; revision requested March 9 and received March 29; accepted May 12. All authors have no financial relationships to disclose. **Address correspondence to** R.B.D. (e-mail: *rdyer@wfubmc.edu*).

1a.

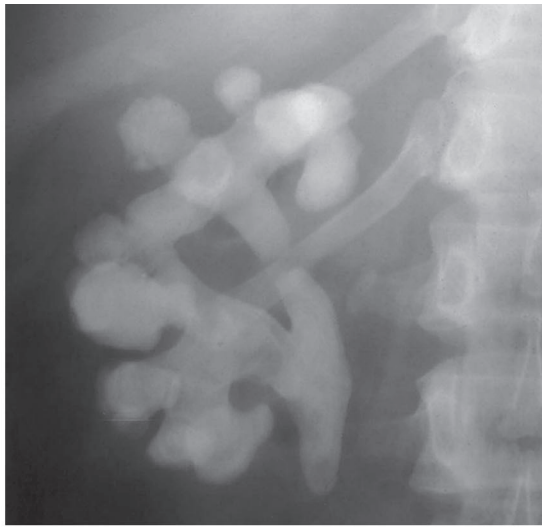

1b.

2a.

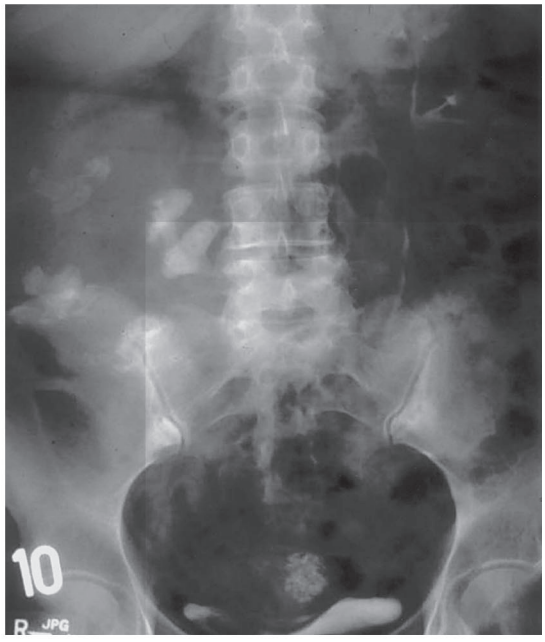

2b.

Figures 1, 2. **(1a)** Staghorns. **(1b)** On a scout image obtained before excretory urography, a calculus fills nearly the entirety of a bifid right renal collecting system, giving it a branched appearance that resembles the antlers of a stag. **(2a)** Scout radiograph obtained before excretory urography demonstrates disruption of the elements of a staghorn calculus—a fragmented staghorn—in an enlarged right kidney. **(2b)** Excretory urogram shows no evidence of contrast material excretion from the right kidney. Renal enlargement, presence of an obstructing stone, and absence of excretion are considered the classic imaging triad of xanthogranulomatous pyelonephritis.

Introduction

Descriptions of observations made from images are the radiologist's stock in trade. Because we "see what we know," any device that aids in the recognition and interpretation of imaging findings is useful. The article reviews "classic signs," often referred to as an "Aunt Minnie," encountered in the urinary tract.

Staghorn and Related Signs

A renal stone described as a *staghorn* implies a branched renal calculus that resembles the antlers of a stag (Fig 1). It is usually composed of struvite; but less commonly, it is formed from cystine

Figure 3. **(a)** A bear's paws. (Photograph entitled "Bad Boys of the Arctic" reprinted with permission from Thomas D. Mangelsen, Inc.) **(b)** Contrast material–enhanced CT scan (same patient as in Fig 2) demonstrates a centrally obstructing stone with replacement of the renal parenchyma by low-attenuation collections in a "hydronephrotic" pattern. Note the lack of dilatation of the renal pelvis and infundibula. **(c)** CT scan obtained at a slightly lower level shows the fragments of a staghorn calculus within the parenchymal collections, which exhibit marginal enhancement. The pattern seen at CT resembles a bear's paw.

a.

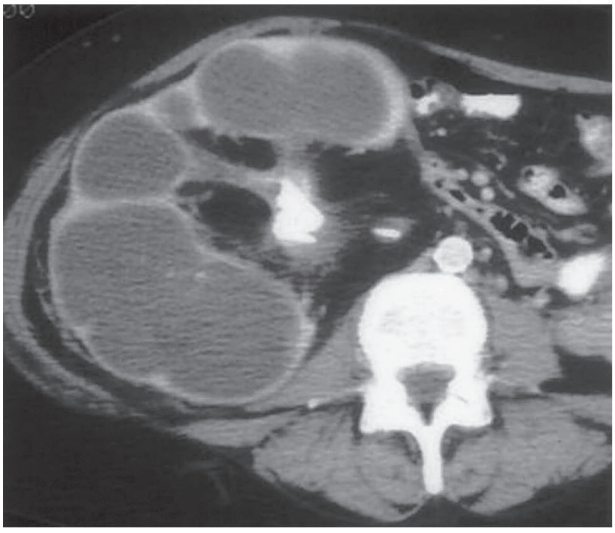

b.

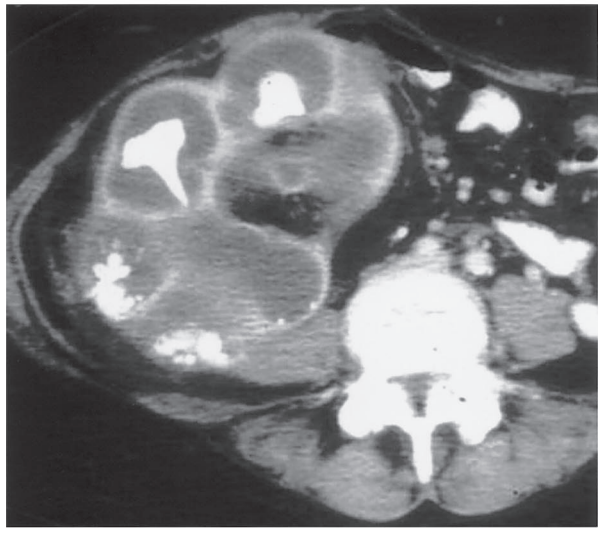

c.

or uric acid. In its most common form, a staghorn renal stone is associated with recurrent urinary tract infections from bacterial pathogens that produce alkaline urine. As such, it is the only type of renal stone that is more commonly seen in women (1).

The staghorn configuration can be disrupted when infection complicates obstruction related to the stone. Renal enlargement from pyonephrosis or xanthogranulomatous pyelonephritis may produce a *fragmented staghorn* (2). In addition to the obstructing stone, which may be fragmented, renal enlargement and nonexcretion of contrast material from the involved kidney constitute the classic excretory urographic triad of xanthogranulomatous pyelonephritis (Fig 2). A stone associated with a nonfunctioning kidney may also be seen with pyonephrosis or long-standing hydronephrosis. CT of xanthogranulomatous pyelonephritis will also illustrate this classic triad. The replacement of the renal parenchyma by the indolent infectious process in the diffuse form of xanthogranulomatous pyelonephritis produces hypoattenuating masses arranged in a "hydronephrotic" pattern, which replaces the renal parenchyma. There may be enhancement in the margins of these masses after contrast material administration. This appearance on CT scans has been described as the *bear paw sign* (Fig 3) (3).

Jack Stone and Other Stone Configurations

Urinary tract stones composed of calcium oxalate dihydrate can assume a spiked configuration, resembling a child's toy jack. Although most commonly seen in the bladder, *jack stones* may

4a.

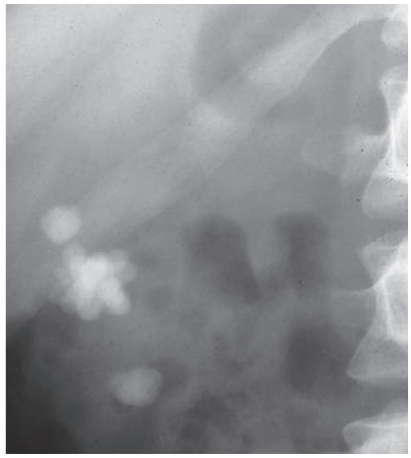

4b.

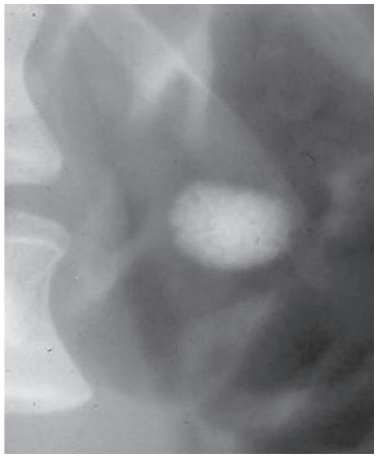

5.

Figures 4, 5. **(4a)** Jacks. **(4b)** Scout radiograph shows a jack stone with long spikes that has formed within the kidney. **(5)** Scout radiograph of a mulberry stone shows its less well-developed spikes, which give it a mamillated appearance, resembling a mulberry.

a.

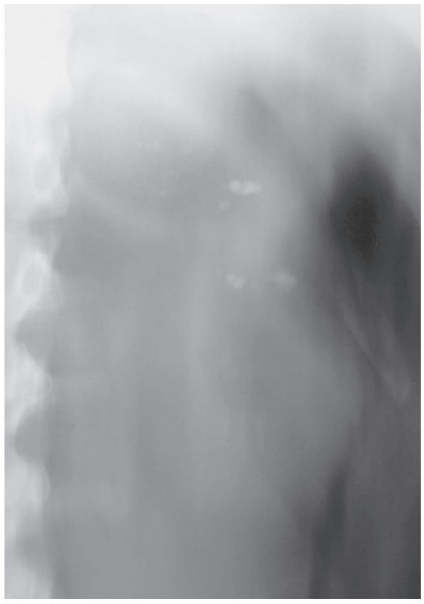

b.

c.

Figure 6. **(a)** "Sponge" kidney, made from a sponge! **(b)** Scout image from excretory urography demonstrates calcifications clustered in the medullary portion of the left kidney. **(c)** After contrast material administration, numerous cavities are identified within the renal papilla in the patient with medullary sponge kidney. Some of the calcifications appear to grow, as contrast agent fills the entire cavity containing the stone.

occasionally form in the kidney (Fig 4). A stone with less well-developed spikes, giving rise to a mamillated appearance, is sometimes referred to as a *mulberry* stone (Fig 5). The loose crystalline lattice of calcium oxalate dihydrate allows these stones to be easily fragmented with various forms of lithotripsy, despite their formidable appearance (1).

Renal Parenchymal Calcification

Thin rims of dystrophic calcification may be deposited at the inner and outer margins of the renal cortex as a result of a major vascular insult that produces cortical necrosis, or rarely, as a consequence of glomerulonephritis, hyperoxaluria, and Alport syndrome, with the development of cortical nephrocalcinosis. The pattern of parenchymal calcification is said to resemble a *tramline* or *railroad tracks* (4).

Medullary nephrocalcinosis is most commonly caused by medullary sponge kidney, renal tubular acidosis, and hyperparathyroidism (1). Medullary *sponge kidney* is the term applied to the development of ectatic tubules occurring in the medullary pyramids (Fig 6) (5,6). As a result of stasis and the occasionally associated condition of hypercal-

a.

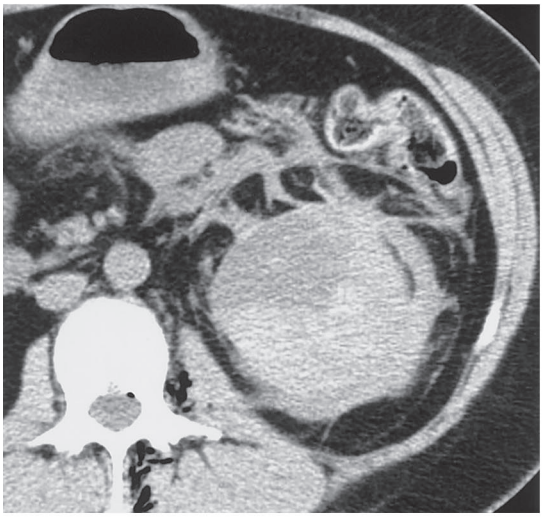

b.

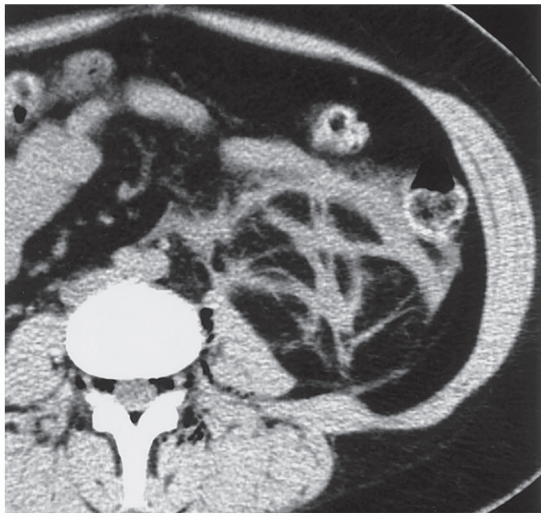

c.

Figure 7. **(a)** Cobwebs. **(b)** CT scan obtained after extracorporeal lithotripsy reveals a subcapsular hematoma and exaggeration of Kunin septa on the left. Renofascial and renorenal septa are especially well identified. **(c)** On another CT scan obtained at the lower aspect of the left kidney, fasciofascial septa are nicely seen, and the cobweb appearance is particularly well developed.

ciuria, stones may form in the cavities, producing medullary nephrocalcinosis. The *growing calculus sign* refers to the apparent enlargement of stones between the preliminary image and images obtained after contrast material administration, as contrast material fills the ectatic tubules harboring the stones (6).

Perirenal Cobwebs

Perirenal cobwebs were initially attributed to collateral vessels seen in the perinephric space in patients with renal vein thrombosis (7). As our ability to image the perinephric space with CT improved, it became clear that a number of disease processes were manifest by development of prominent perinephric structures (8). Kunin (9) formalized our understanding by describing several types of septa that compartmentalize the perirenal space and that may confine, or act as a conduit for, extension of a disease process (Fig 7).

Currently, perirenal cobwebs (visualization of perirenal septa) are most frequently encountered during the CT evaluation of urinary tract obstruction from stone disease. Perirenal stranding, occurring in the setting of flank pain from ureteral colic, is an exaggeration of the visibility of these septations due to edema and fluid extravasation, and is an important secondary sign of acute ureteral obstruction from stones (10). Perirenal stranding in the asymptomatic patient is often a nonspecific finding and may be seen in benign and malignant conditions.

Soft-Tissue Rim Sign

The CT evaluation of stone disease has given rise to new signs. The *soft-tissue rim sign* is caused by edema of the ureteral wall surrounding a stone at

a. b.

Figure 8. **(a)** One kind of rim (with thanks to Christopher R. Dyer for his assistance with this photograph.) **(b)** CT scan shows a thin soft-tissue rim (arrow) surrounding a stone impacted in the middle of the left ureter. The rim represents edema of the ureteral wall. The presence of a tissue rim sign allows a confident diagnosis of a stone within the ureter.

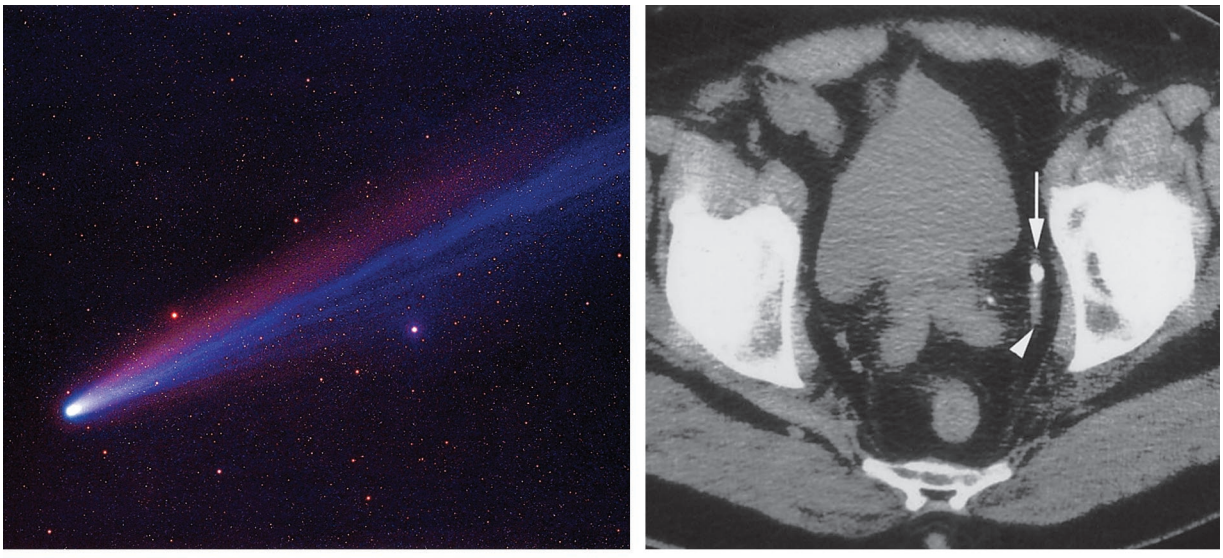

a. b.

Figure 9. **(a)** Comet. (Photograph entitled "Comet Hyakutake" reprinted with permission from Bill and Sally Fletcher.) **(b)** CT scan shows a calcification (the comet nucleus) (arrow) with a soft-tissue tail that represents a pelvic vein (arrowhead). Together, this appearance constitutes the comet sign. Note the stone at the left ureterovesical junction.

its site of impaction (Fig 8) (11). The importance of the sign lies in the fact that it may help to distinguish a stone in the ureter from a phlebolith in an adjacent vein, because the occurrence of a soft-tissue rim around a phlebolith is uncommon. It should be noted, however, that the soft-tissue rim sign may be absent with stones larger than 4 mm or when a stone is impacted at the ureterovesical junction.

Comet Sign

The *comet sign* (Fig 9) has also been used at CT to aid in the differentiation of a phlebolith from a stone in the ureter, especially in the anatomic pelvis (12). The calcified phlebolith represents the comet nucleus and the adjacent, tapering, noncal-

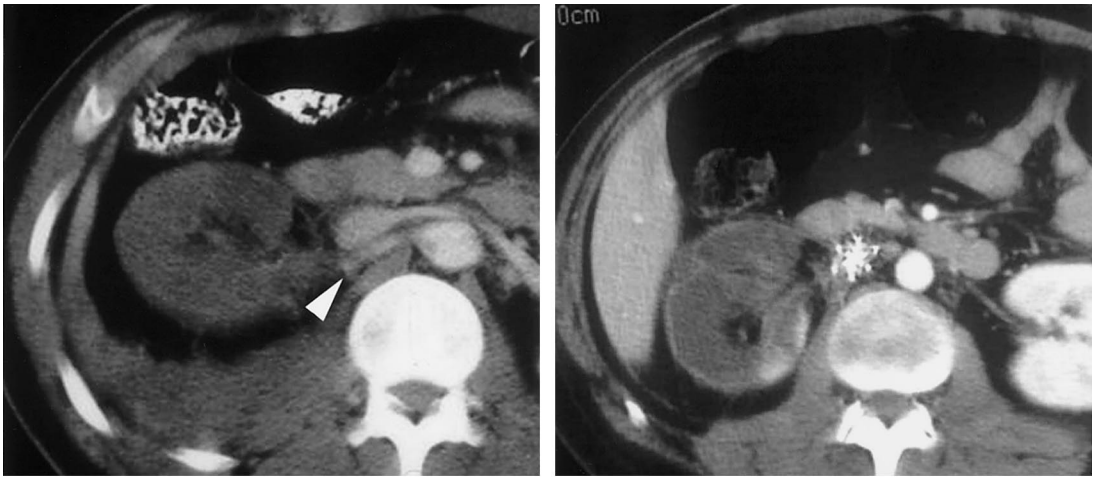

a. **b.**

Figure 10. Rim sign of vascular compromise. **(a)** Enhanced CT scan of a motor vehicle accident victim demonstrates no perfusion in the majority of the right kidney. The right renal artery abruptly terminates; this is the arterial cut-off sign (arrowhead). **(b)** Repeat contrast-enhanced CT scan, obtained 72 hours after **a**, demonstrates a thin marginal rim of preserved subcapsular enhancement in the left kidney, typical of the rim sign of renovascular compromise. Vascular compromise in this case was caused by intimal injury and thrombosis of the main renal artery.

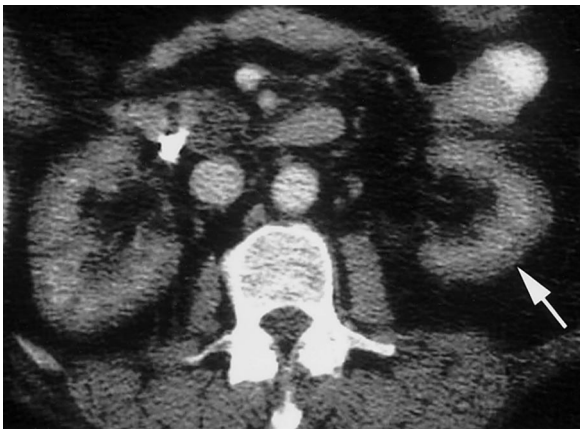

Figure 11. A reverse rim. CT scan, obtained to exclude a large retroperitoneal hematoma in a patient with sustained hypotension for 1 hour after cardiac catheterization and subsequent cardiac arrest, shows a hypoattenuating renal cortex (arrow) compared with the medullary enhancement. No additional contrast material was given after the catheterization. The patient rapidly developed multiorgan failure that led to her death.

cified portion of the vein is the comet tail. The reliability of the comet sign is not as great as that for the soft-tissue rim sign, however.

Other Rims

A very important rim sign with an entirely different cause is that associated with major vascular compromise in the kidney. This sign is most commonly seen with renal artery obstruction from thrombosis, embolus or dissection. At contrast-enhanced CT or MR imaging, a 1- to 3-mm rim of subcapsular enhancement, paralleling the renal margin, can be seen as a result of preserved perfusion of the outer renal cortex by capsular perforating vessels. The finding may be partial or total depending on the level of vascular occlusion, and there may be an abrupt termination of contrast material in the renal artery referred to as the *arterial cut-off sign* (Fig 10) (13,14). The *rim sign of vascular compromise* has also been described with renal vein thrombosis and acute tubular necrosis (13).

The *reverse rim sign* refers to a hypoattenuating renal cortex visualized at CT, seen against a background of intact medullary perfusion after contrast material is given. This sign also implies severe derangement of cortical blood flow with development of cortical necrosis (Fig 11) (15). Cortical necrosis may develop as a consequence of obstetric complications, shock from numerous causes, transfusion reaction or other causes of intravascular hemolysis, toxins, and rejection in the transplanted kidney (16).

A different type of rim sign can be seen in association with chronic hydronephrosis. After contrast material is administered, enhancement occurs in the residual, but markedly atrophic, renal parenchyma, surrounding the dilated calices and renal pelvis. The inner margin of this *hydronephrotic rim* is concave toward the renal hilum, and enhancement of the cortical columns between the dilated collecting system elements may be seen. This type of rim has been observed in all forms of

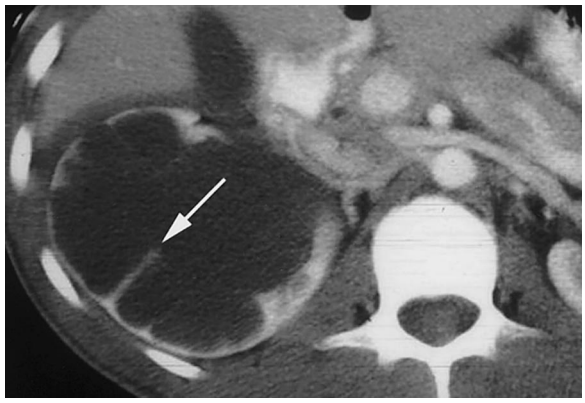

Figure 12. Hydronephrotic rim. CT scan, obtained in a patient with hematuria after minimal trauma, reveals a rim of enhancement surrounding a markedly dilated right renal pelvis and collecting system, findings consistent with congenital ureteropelvic junction obstruction. Note the variable thickness of the enhancing tissue rim (in contrast to the rim sign of vascular compromise [cf Fig 10]), as well as enhancement within cortical columns (arrow).

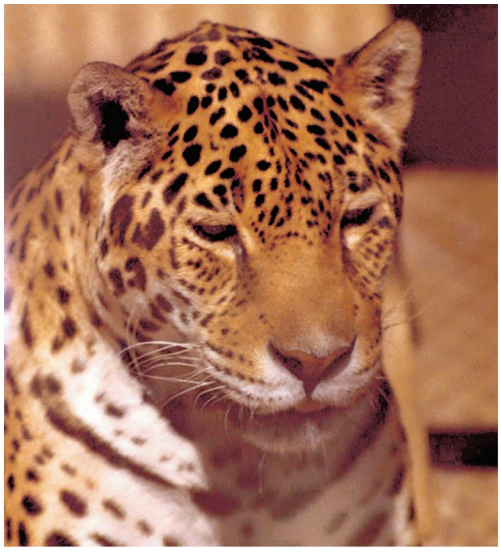

13a.

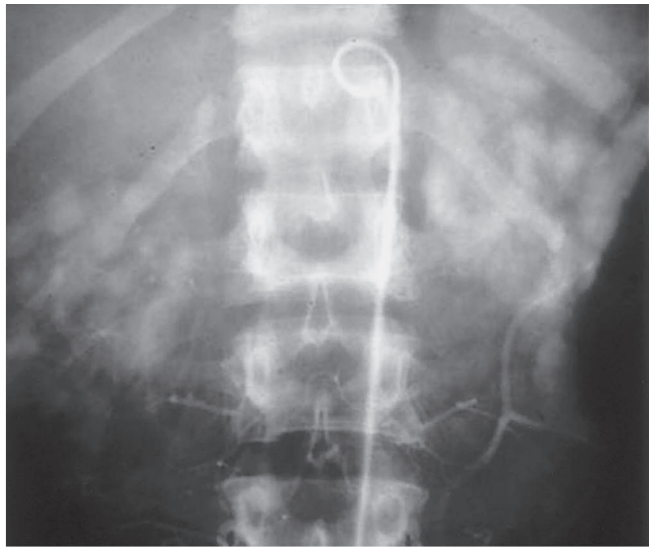

13b.

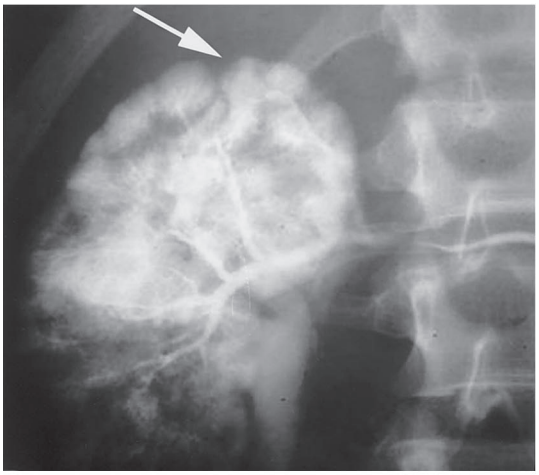

13c.

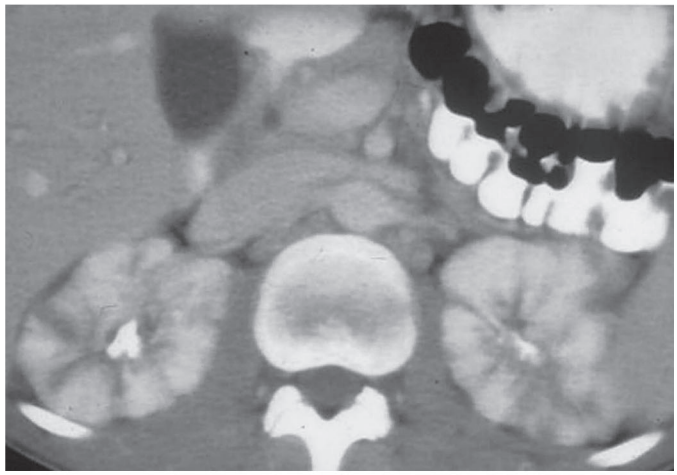

14.

Figures 13, 14. Spotted nephrogram. **(13a)** Spotted cat. (Courtesy of Russell I. Poole, Mishawaka, Ind.) **(13b)** Late image from midstream aortography demonstrates patchy perfusion in both kidneys, giving the parenchyma a spotted appearance: the spotted nephrogram. **(13c)** Late image from selective right renal arteriography in the same patient demonstrates small vessel occlusion and multiple areas of parenchymal infarction (arrow) with islands of preserved perfusion. The patient proved to have periarteritis nodosa. **(14)** CT scan of another patient with periarteritis nodosa demonstrates the CT correlate of the angiographic findings, with patchy perfusion of the kidneys caused by multiple areas of infarction. (Case courtesy of N. Reed Dunnick, MD, University of Michican Health System, Ann Arbor, Mich.)

a.

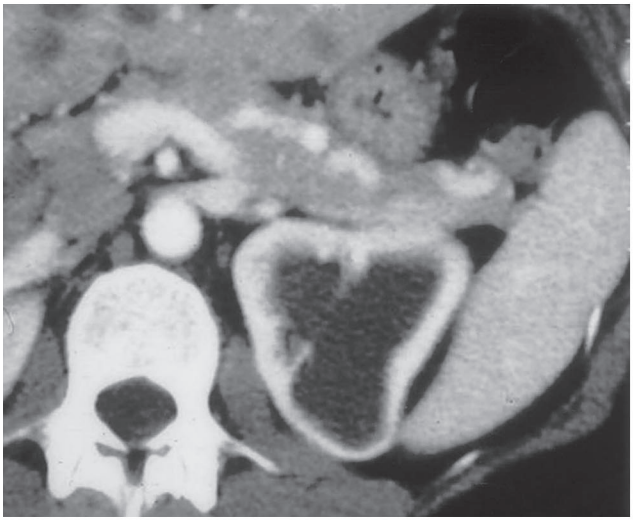

b.

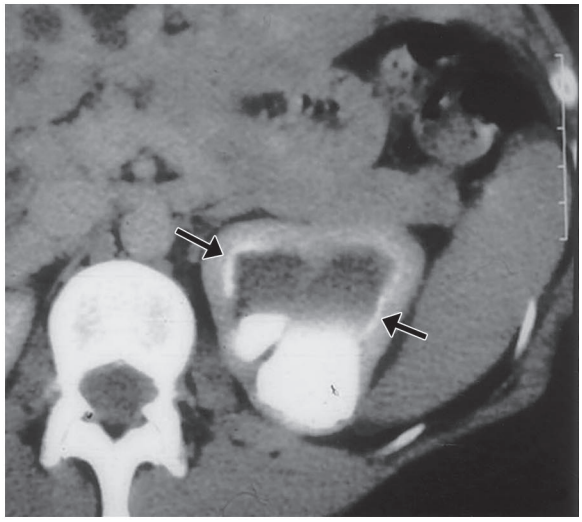

c.

Figure 15. **(a)** Crescent. (Photograph entitled "Moon with Earthshine" reprinted with permission from Bill and Sally Fletcher.) **(b)** Crescent sign. CT image obtained during the corticomedullary phase of enhancement shows decreased thickness of the parenchyma surrounding the dilated collecting system in the left kidney. **(c)** Concentrated contrast material crescents surround the dilated collecting system elements (arrows) on this delayed image, which also shows a urine–contrast agent level in the dependent aspect.

contrast-enhanced imaging of the obstructed kidney (Fig 12). Unopacified urine in the dilated collecting system may produce a *negative pyelogram*. Depending on the degree of residual excretory function, delayed imaging may show pools of contrast material or a urine–contrast material level within the distended collecting system (17).

Spotted Nephrogram

Irregular, patchy enhancement in the renal parenchyma, referred to as the *spotted nephrogram*, may occur as a result of small vessel occlusion, which can be seen with necrotizing vasculitis (periarteritis nodosa), scleroderma, and hypertensive nephrosclerosis (18). Although first observed on angiograms (Fig 13), the abnormal perfusion pattern can be identified on CT (Fig 14) and MR images after contrast material administration (19).

Crescent Sign

This sign is fundamentally different in its pathophysiology from the rim sign of hydronephrosis. The *crescent sign* refers to the appearance of concentrated contrast material in collecting tubules, arranged parallel to the margin of a dilated calix, which produces a thin line of contrast material at the edge of the calices, resembling a crescent (Fig 15). This change in tubule orientation from vertical to near horizontal, at the margin of the calix, is related to prolonged, but often incomplete, obstruction that produces gradual dilatation of the collecting system (20,21). The sign is important because it indicates that renal function within the kidney is recoverable, despite the severity of collecting system dilatation.

a. b. c.

Figure 16. **(a)** Balloon on a string (with thanks to Richard T. Dyer for his help with this photograph). **(b)** Balloon on a string sign. Delayed tomographic image from excretory urography shows caliceal crescents (arrowheads) surrounding the dilated collecting system. Contrast material pools dependently. **(c)** Image from retrograde ureteropyelography, performed after several weeks of ureteral stent placement, shows an eccentric exit of the ureter from the dilated renal pelvis. This appearance resembles a balloon on a string and is typical of ureteropelvic junction obstruction.

Balloon on a String Sign

The *balloon on a string sign* may be seen with the rim sign of hydronephrosis, with the crescent sign, or as an isolated finding. This sign refers to the appearance of a high and somewhat eccentric exit point of the ureter from a dilated renal pelvis and is a typical finding of ureteropelvic junction obstruction (Fig 16) (22). The possibility of an associated crossing vessel should always be evaluated before therapeutic intervention.

Concentric Ring Sign (Target Sign) and Kidney Sweat

MR imaging may reveal a *concentric ring* or *target* pattern of hyper- and hypointensity within hematomas that have been present for more than 3 weeks (23). The ring pattern is best seen on T1-weighted images (Fig 17). The peripheral dark rim is likely related to pseudocapsule development. An inner bright ring is thought to be caused by hemoglobin degradation, whereas a central core of intermediate, but variable, intensity is related to the age of the hematoma (23).

An extracapsular, hypoechoic rim of simple-appearing fluid surrounding the kidneys, first described at ultrasonography (US) in some patients with renal failure, was called *kidney sweat* (Fig 18) (24). These collections can also be identified at CT and MR imaging (Fig 19). The rim is thought to represent perirenal edema, and recognition of this sign should prevent confusion with more significant perirenal fluid collections, such as hematoma or abscess.

a.

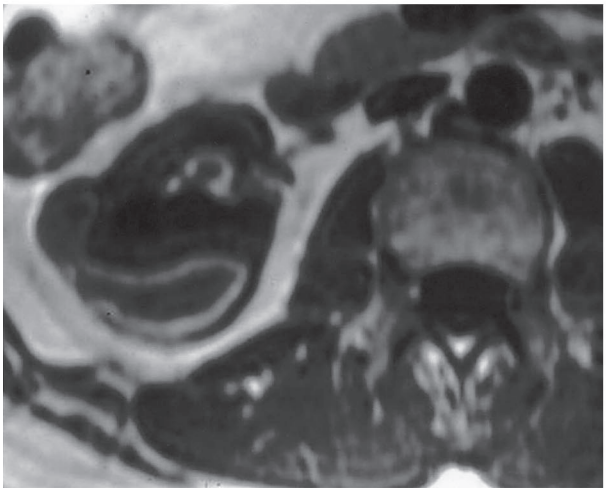

b.

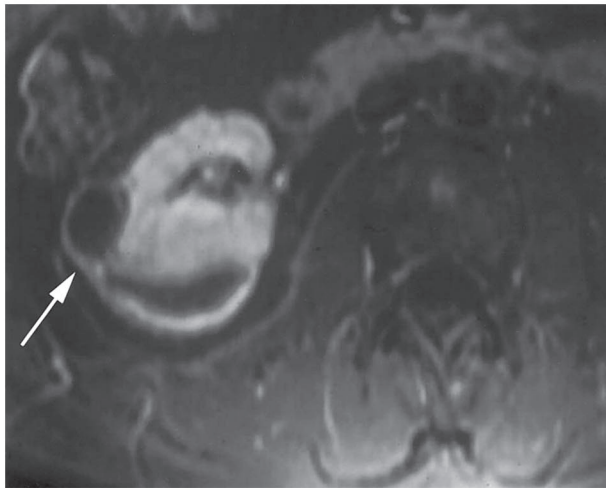

c.

Figure 17. **(a)** Target sign (registered trademark of Target, Inc.). **(b)** T1-weighted MR image of the right kidney shows a subcapsular collection with a target appearance, a finding indicative of hemoglobin degradation in a subacute hematoma. **(c)** Gadolinium-enhanced, fat-suppressed T1-weighted MR image reveals that the source of the hemorrhage was a papillary renal cell carcinoma (arrow).

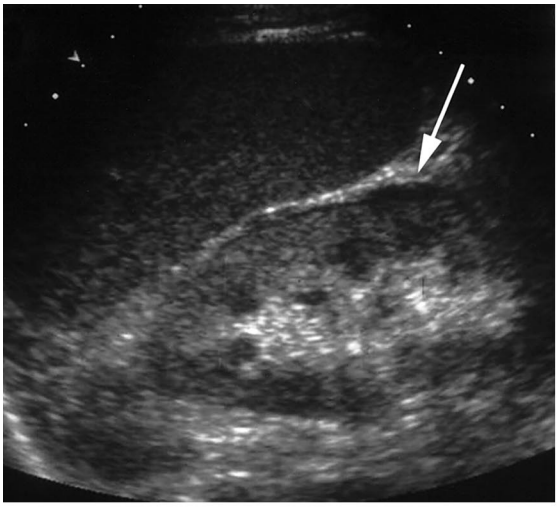

18.

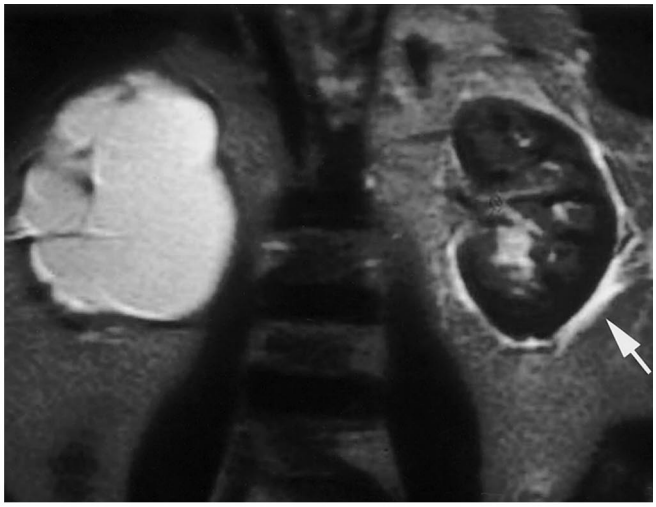

19.

Figures 18, 19. Kidney sweat. **(18)** Longitudinal US image of the left kidney in a patient with acute renal failure reveals a sliver of fluid in a subcapsular location (arrow). This appearance has been called kidney sweat. Similar findings were seen on the right. **(19)** In another patient with acute renal failure, the T2-weighted MR image shows kidney sweat on the left (arrow). A balloon on a string appearance is seen in the right kidney, which had no excretory function because of severe parenchymal atrophy.

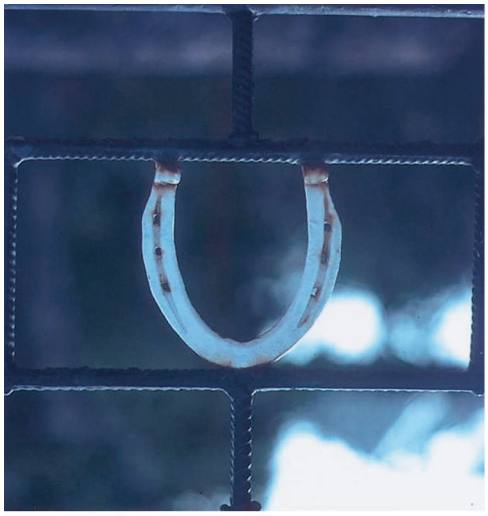

20a.

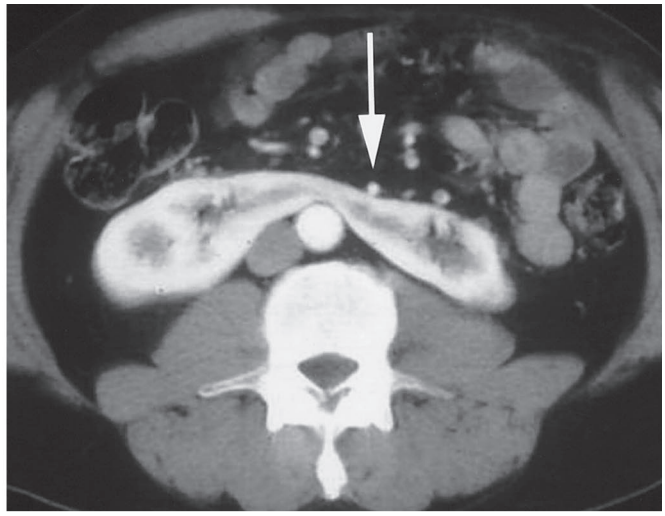

20b.

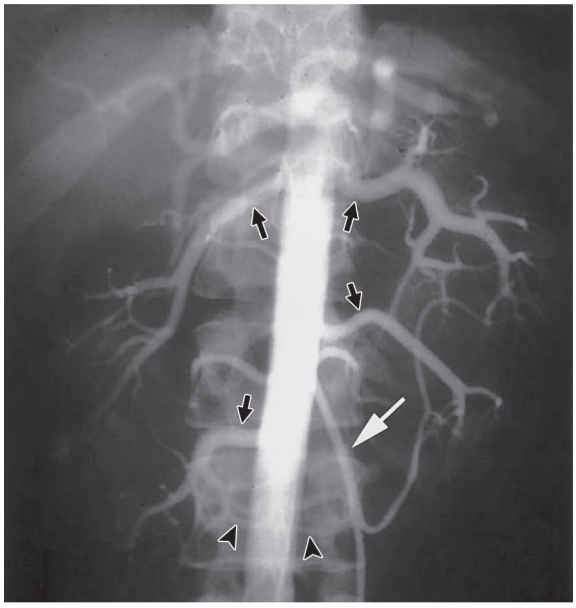

21a.

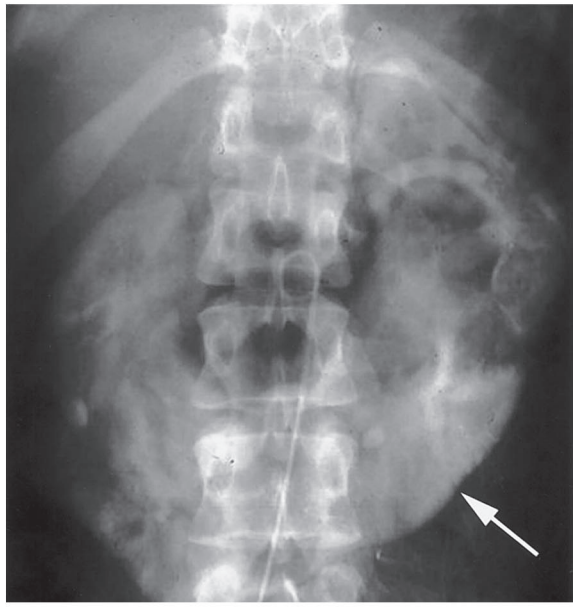

21b.

Figures 20, 21. Horseshoe kidney. **(20a)** Horseshoe. **(20b)** Enhanced CT image shows the functional isthmus of a horseshoe kidney anterior to the aorta, immediately beneath the inferior mesenteric artery (arrow). **(21a)** Midstream aortogram demonstrates multiple renal arteries supplying a horseshoe kidney (black arrows and arrowheads). Note the position of the inferior mesenteric artery (white arrow). **(21b)** Late phase image from aortography demonstrates the horseshoe kidney configuration (arrow), with the superior aspect of the isthmus immediately below the origin of the inferior mesenteric artery.

Horseshoe Kidney and Other Fusion Anomalies

Horseshoe describes the shape of the most common congenital renal fusion anomaly, occurring in approximately one in 400 live births (25). Fusion of the lower renal poles, which produces an isthmus of tissue crossing the midline anterior to the aorta, has a number of consequences. The isthmus is an impediment to normal rotation and upward ascent as it encounters the inferior mesenteric artery (Fig 20). Routinely, the vascular supply to these *horseshoe kidneys* will be anomalous (Fig 21). The rotational anomalies and transit of the isthmus by the ureters can result in varying degrees of obstruction of the renal moieties, with an increased prevalence of stone formation and infection (25). The horseshoe kidney can be associated with a variety of other congenital anomalies including vertebral, anorectal, tracheal, and esophageal malformations. Other fusion anomalies may be encountered including a wide variety of crossed-fused ectopic kidneys, the *disc* (*pancake*) kidney, and pelvic *lump* (*cake*) kidney. Patients with these types of kidneys suffer similar complications (25).

a.

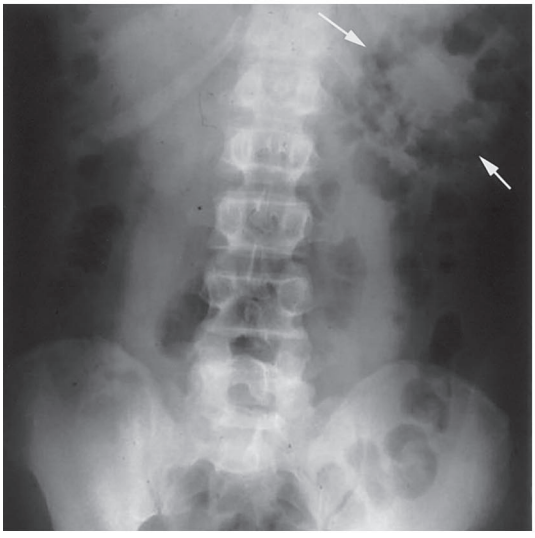

b.

c.

Figure 22. **(a)** One kind of loop-to-loop. **(b)** Preliminary image from excretory urography demonstrates a looped configuration of the distal transverse colon and splenic flexure (arrows). **(c)** Tomogram from excretory urography demonstrates absence of the left kidney and deviation of the descending colon into the renal fossa.

Loop-to-Loop Colon and the Lying Down (Pancake) Adrenal Gland

A normal kidney in a normal position is the foundation for image interpretation of many of the anticipated anatomic relationships. The *loop-to-loop colon* describes an abnormal colonic course associated with the absence of the left kidney from the renal fossa. The transverse colon extends to the lateral margin of the abdominal wall, and the descending colon courses medially to fill the renal fossa, resulting in the looped colonic configuration (Fig 22) (26). The presence of large intestine in the renal fossa at imaging should lead to a consideration of renal agenesis or ectopia.

Similarly, the typical radiologic appearance of an inverted Y-shaped, V-shaped, or wishbone-shaped adrenal gland depends, in part, on the presence of a kidney in the renal fossa. With renal agenesis, the ipsilateral adrenal gland will be present in the majority of cases, but the configuration of the gland, especially if it is on the left side, may assume a long slender pancake or disc shape that has been described as *lying down* (Fig 23) (27).

Lumps, Bumps, and Dromedary Humps

Normal tissue can appear as a variety of pseudomasses in the kidney. Renal tissue molded by adjacent organs, most commonly the spleen affecting the left kidney, may create a prominent mass

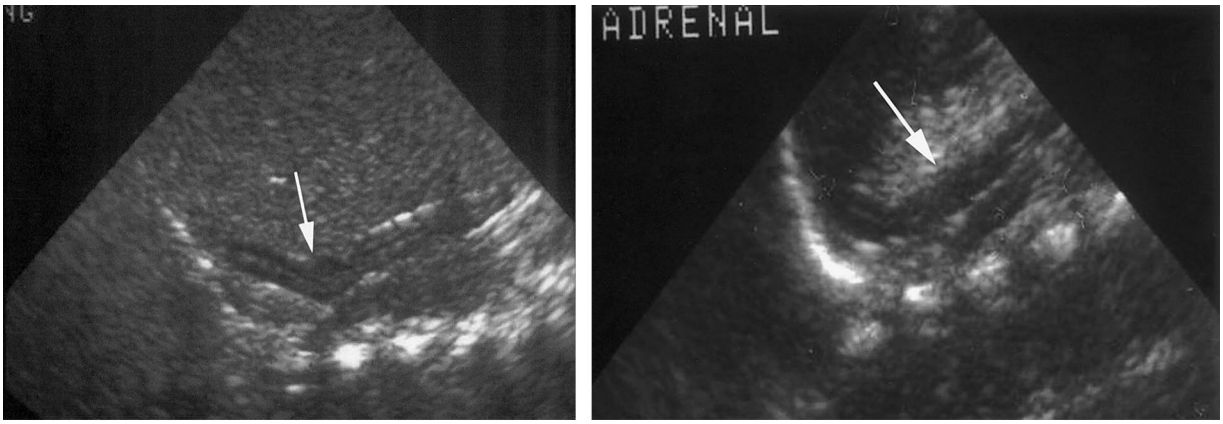

a. b.

Figure 23. Lying down adrenal glands. US images of the right **(a)** and left **(b)** renal fossae demonstrate absence of the kidneys, and long, slender adrenal glands (arrows) in an infant with bilateral renal agenesis.

a. b.

c.

Figure 24. **(a)** Dromedary camel (registered trademark of R. J. Reynolds Tobacco Co.). **(b)** Dromedary hump. Tomogram from excretory urography demonstrates a prominent cortical hump in the interpolar region of the left kidney. **(c)** On a compression image obtained in a later phase of the sequence, the hump is subtended by a normal collecting system element, indicating that it represents normal functioning tissue.

referred to as a *dromedary hump* (Fig 24) (28). The appearance of this tissue should have the signature of normal renal parenchyma, regardless of the type of imaging study performed. Most important, the area should be subtended by a normal collecting system element, and a normal interpapillary line should be present. Prominent cortical columns, suprahilar lips, and persistent fetal lobation may also produce confusing appearances at imaging studies with the potential for misdiagnosis for those who are unaware (Fig 25) (25,28–30).

Putty Kidney and Other Signs Associated with Urinary Tract Tuberculosis

As an end stage of infection with tuberculosis in the genitourinary tract, calcification may entirely outline a nonfunctional kidney. The radiologic appearance of this condition, which is associated with autonephrectomy, has been described as the *putty kidney* (Figs 26, 27) (31,32). Calcification

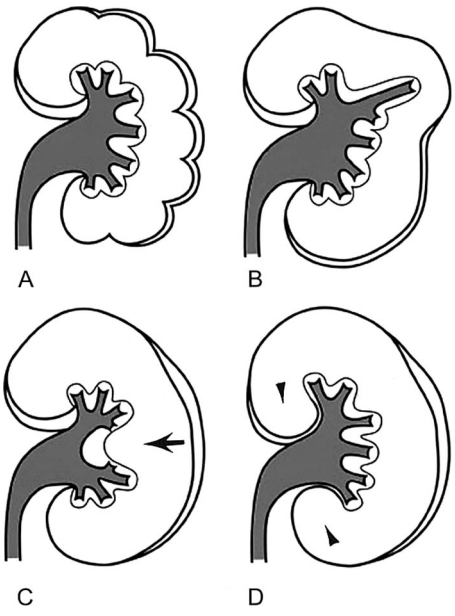

Figure 25. Drawings illustrate a variety of pseudomasses that can be created by normal renal tissue: fetal lobation *(A)*, dromedary hump *(B)*, cortical column (arrow) *(C)*, and prominent hilar lips (arrowheads) *(D)*. Familiarity with the typical locations and appearances of pseudomasses aids in the correct diagnosis.

26a.

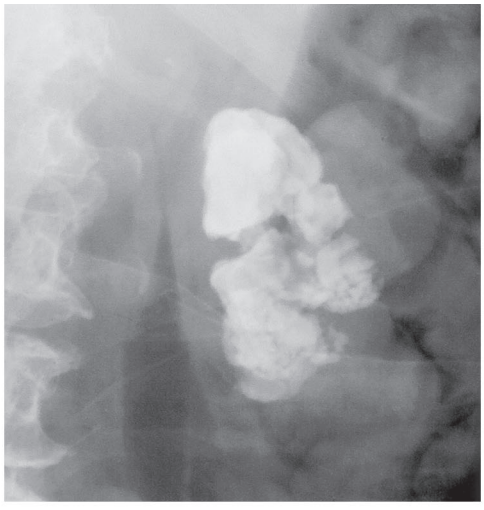

26b.

27a.

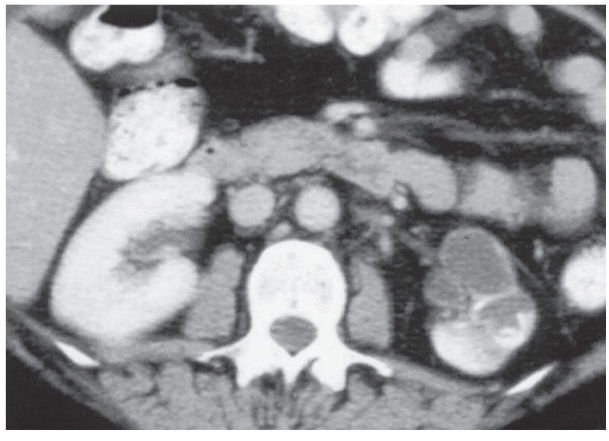

27b.

Figures 26, 27. Putty kidney. **(26a)** Putty kidney. **(26b)** Plain radiograph of the abdomen demonstrates extensive calcification in the left kidney, which was nonfunctional (the putty kidney), consistent with autonephrectomy from tuberculosis. **(27)** CT images through the upper **(a)** and lower **(b)** regions in another patient with autonephrectomy of a left-sided, putty kidney demonstrate the extensive parenchymal and collecting system calcification as a result of tuberculosis infection.

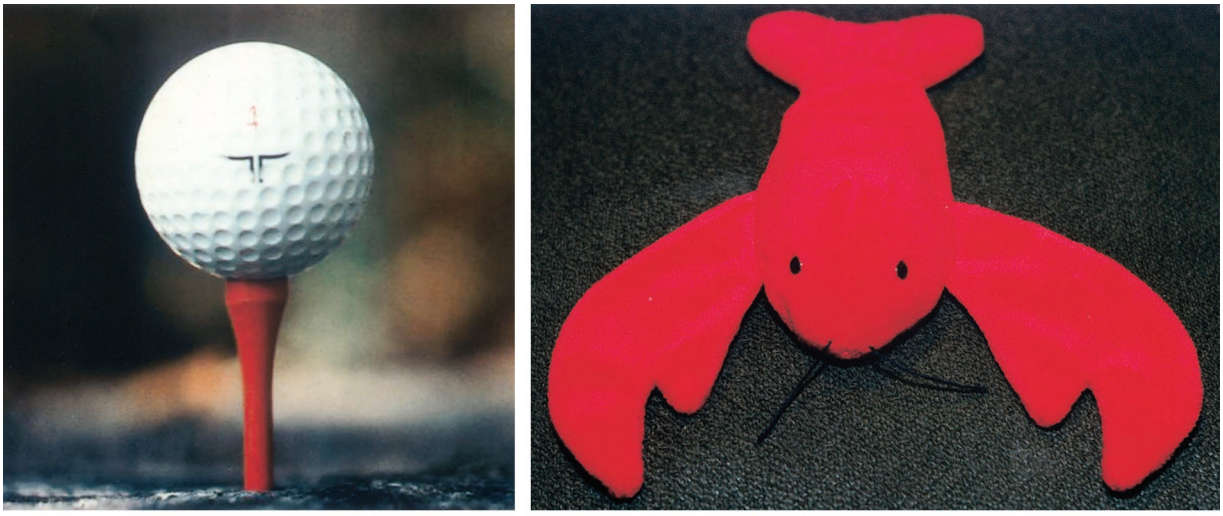

a. b. c.

Figure 28. **(a)** Ball-on-tee. **(b)** Lobster claws with lobster. **(c)** Drawing illustrates the different patterns of excavation that can be seen with papillary necrosis: normal *(A)*, central excavation with ball-on-tee appearance *(B)*, forniceal excavation *(C)*, lobster claw appearance *(D)*, signet ring appearance *(E)*, and sloughed papilla with clubbed calix *(F)*.

may also be seen in other portions of the urinary tract as a consequence of tuberculosis infection. Following reactivation of hematogenously disseminated disease, irregularity of the caliceal margin, which is sometimes referred to as a *moth-eaten* appearance, may be the first recognizable excretory urographic finding of urinary tract tuberculosis. As these areas coalesce, frank papillary cavitation can be identified, with an appearance similar to that of papillary necrosis. As the infection gains access to the collecting system and ureter, a variety of metaphorical terms have been used to describe the imaging findings. Infundibula may be strictured or *amputated*. An involved calix may not be opacified at excretory urography, producing a *phantom calix* (described later). Distortion of the renal pelvis because of stricturing and retraction has been described as a *hiked-up* or *purse-string* appearance. Tuberculosis involvement of the ureter is initially heralded by dilatation and ragged irregularity of the lumen, referred to as a *sawtooth* appearance. Later, the ureter may become a straight rigid tube, referred to as a *pipestem* ureter. Healing with associated fibrosis may also produce a *beaded* or *corkscrew* ureter. Tuberculosis involvement of the bladder may cause calcification in the wall, which may become thick and reduce the capacity of the bladder; the resultant, very small bladder has been referred to as a *thimble* bladder (31,32).

Ball-on-Tee, Lobster Claw, and Signet Ring Appearances

The descriptive terms *ball-on-tee, lobster claw,* and *signet ring* refer to the radiographic patterns of papillary excavation seen with papillary necrosis (Fig 28) (33,34). The necrotic papillary tip may remain within the excavated calix, producing the *signet ring sign* when the calix is filled with contrast material. The devitalized papilla may act as a nidus for calcification, thus creating a true "stone" for the signet ring. The patterns of papillary excavation are best seen with standard excretory urography or retrograde urography (Figs 29–31). Papillary necrosis is usually the result of an ischemic injury to the medullary portion of the kidney and is most often associated with use of *N*onsteroidal anti-inflammatory drugs; *S*ickle cell anemia; *A*nalgesic nephropathy; *I*nfection, especially tuberculosis; and *D*iabetes mellitus (the capitalized, italicized letters create the memory aid NSAID) (33).

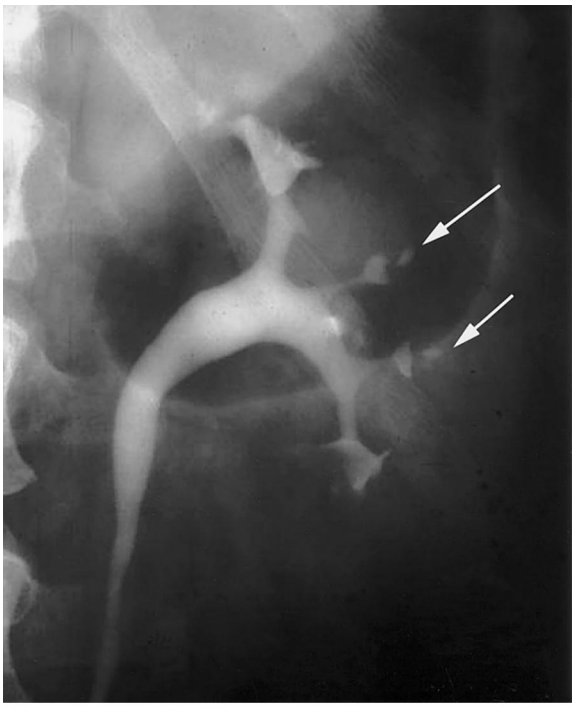

29.

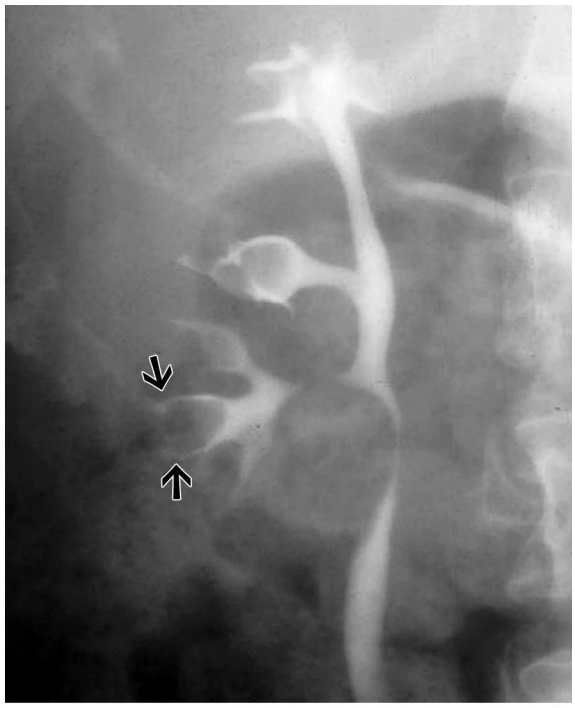

30.

31a.

31b.

Figures 29–31. Papillary necrosis. **(29)** On an excretory urogram, contrast material fills central excavations (arrows) in the papilla of the interpolar region, giving the ball-on-tee appearance. Note the abnormal calices in the upper and lower poles as well. **(30)** Excavation extending from the caliceal fornices (arrows) produces the lobster claw deformity in another patient. **(31a)** Tomogram demonstrates triangular, peripherally calcified structures (arrows)—the sloughed papilla—in the region of the left ureter. **(31b)** Retrograde ureteropyelogram demonstrates contrast material surrounding sloughed papilla retained in some of the calices, producing the signet ring appearance (arrows).

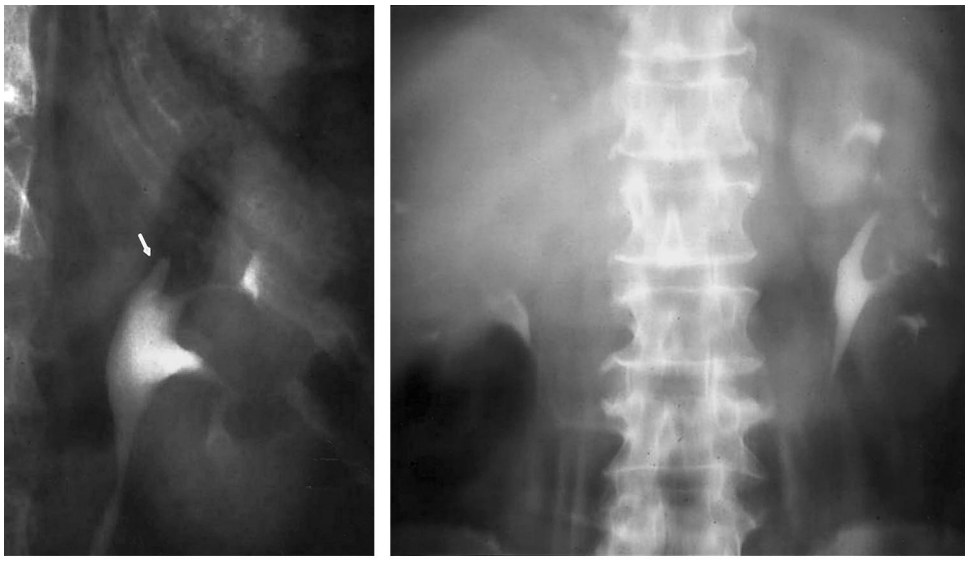

Figure 32. Phantom calix. **(a)** On an excretory urogram, stricturing of the superior infundibulum caused by tuberculosis has obliterated the upper calix (arrow), producing a phantom calix. **(b)** On image of another patient, a mass in the upper pole of the right kidney has destroyed the caliceal elements normally seen in this region. In this case, the phantom calices are secondary to renal cell carcinoma.

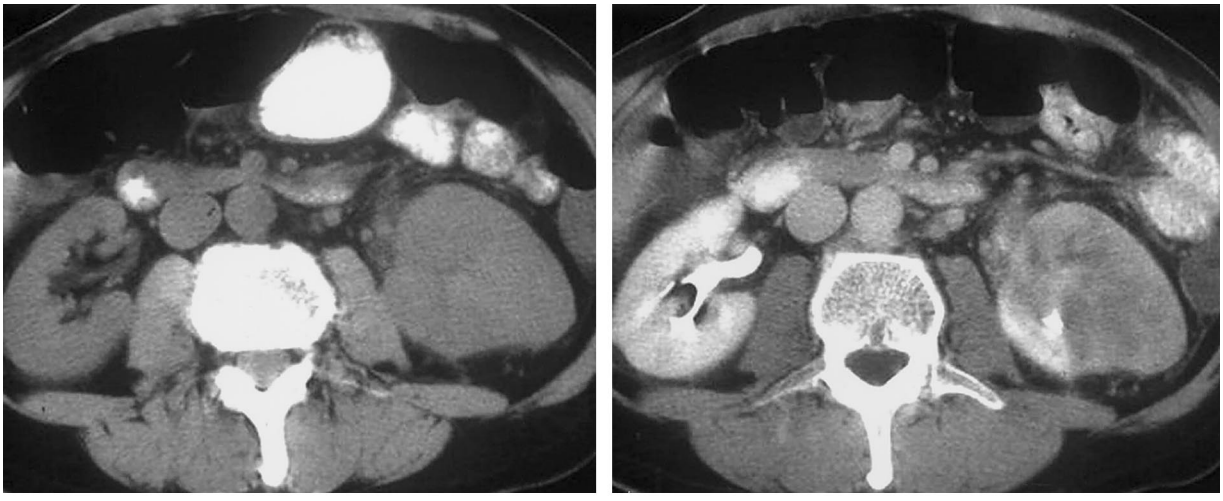

Figure 34. Faceless kidney. **(a)** Unenhanced CT image shows absence of the central sinus signature in the left kidney. Note perinephric stranding and abnormalities in the hilar region. **(b)** Enhanced image obtained at the same level as **a** shows abnormal parenchymal enhancement, in this case from a diffusely infiltrating transitional cell carcinoma.

Phantom Calix

The *phantom calix sign* refers to images of the kidney in which no collecting system element can be identified where one should be found. This finding usually reflects an intrarenal process that has infiltrated and obliterated the collecting system element. The differential diagnosis for this finding includes inflammation (especially tuberculosis and occasionally acute pyelonephritis), neoplasm (especially transitional cell carcinoma), a stricture from trauma or stone passage, ischemia, a congenital anomaly of the calix, renal contusion, or technical underfilling (Fig 32) (35).

Faceless Kidney

The term *faceless kidney* was originally reported as a CT sign of renal duplication (36). In this setting, *faceless* refers to the appearance of the kidney on a CT section obtained at a level between duplicated collecting system elements; at this level, the kidney is entirely filled by normal renal parenchymal tissue, thus lacking the typical familiar signature of central renal sinus structures and sinus fat (Fig 33). Use of the term has been broadened to include any process that obliterates the anticipated sinus appearance of the kidney. Thus, edema from inflammatory conditions or a more "sinister" infiltrative process such as lymphoma or transitional cell carcinoma may render the kidney *faceless* (Fig 34). The familiar "face" should

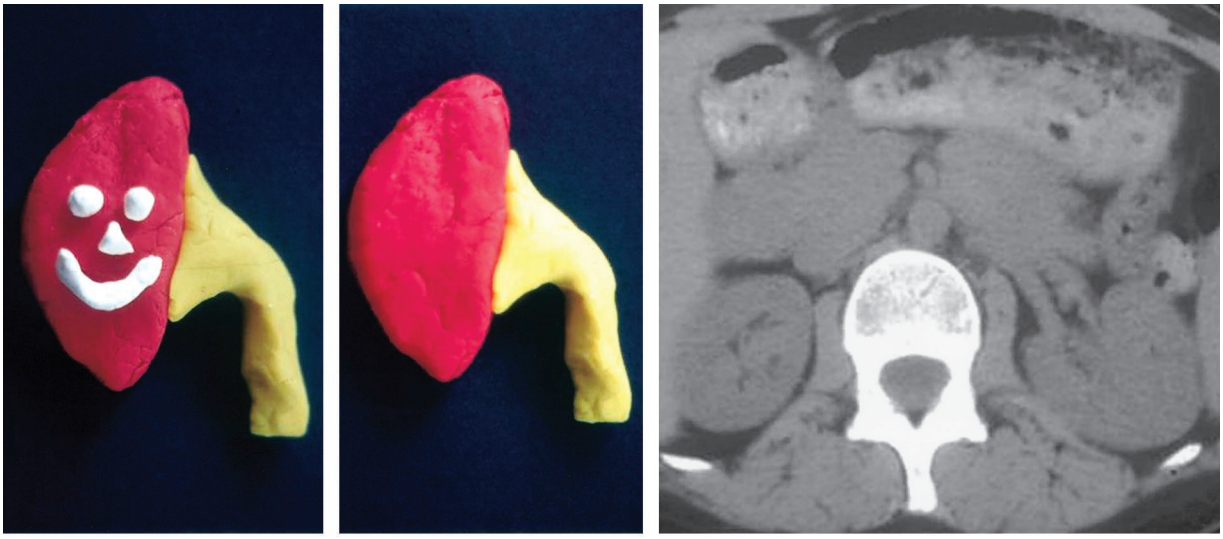

a. b. c.

d.

e.

f.

Figure 33. Faceless kidney sign. **(a, b)** Kidney with **(a)** and without **(b)** a face. **(c)** Unenhanced CT image through the kidneys shows absence of the typical sinus signature in the left kidney. **(d)** Contrast-enhanced image, obtained at the same level as seen in **c,** shows normal parenchymal enhancement. **(e)** Delayed image obtained at the lower aspect of the left kidney shows the presence of two ureters (arrowheads). **(f)** Excretory urogram demonstrates duplication of the left collecting system, with the two separate collecting system elements and two ureters exiting the kidney. It is easy to see how the images in **c** and **d** were generated from a position between the collecting system elements.

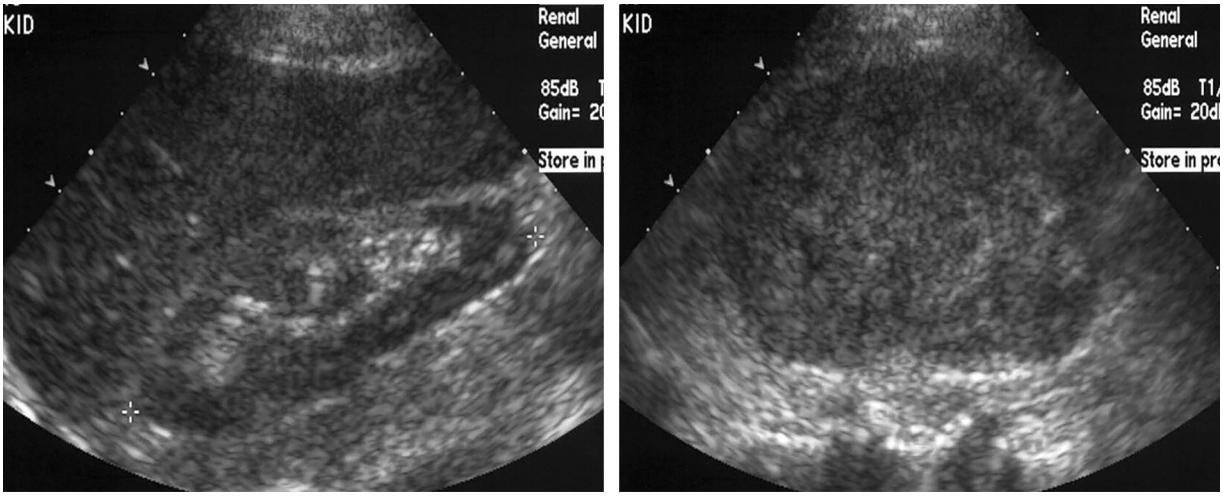

a. **b.**

Figure 35. Faceless kidney. **(a)** US image of the right kidney (same patient as in Fig 34) shows the normal sonographic signature of the renal sinus. **(b)** Sonographic sinus signature in the left kidney is grossly distorted due to infiltration by transitional cell carcinoma.

a. **b.**

Figure 36. **(a)** Drooping lily. **(b)** Excretory urogram of an infant with a urinary tract infection demonstrates downward and lateral displacement of the opacified lower pole moiety of a duplicated system (the drooping lily appearance) caused by the dilated, obstructed collecting system and ureter of the nonfunctional upper pole moiety.

always be present, regardless of the imaging technique used. Its absence or distortion requires explanation (Fig 35).

Drooping Lily Sign

At urography, a dilated, obstructed upper moiety ureter, in a completely duplicated system, may produce downward and lateral displacement of the functional lower moiety collecting system, appearing radiographically as the well-known *drooping lily sign* (Fig 36) (37,38). The sign is often accompanied by a bladder filling defect, representing a ureterocele, which is associated with the ectopic insertion of the upper moiety ureter. As the frequency of excretory urography wanes, the "classic" drooping lily is less frequently encountered. Diagnostic consideration should be given to the presence of a duplication anomaly whenever a process is discovered in only one portion of a kidney (37).

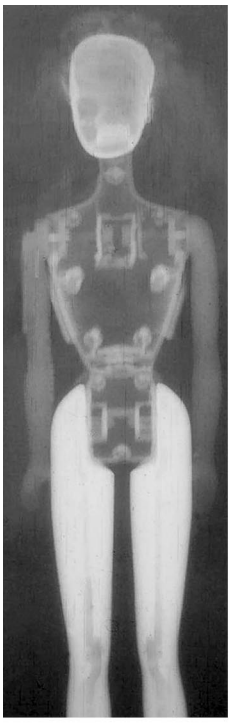

37a.

37b.

Figures 37, 38. **(37)** Maiden waist deformity. **(a)** Radiograph of Barbie (registered trademark of Mattel) clearly depicts a narrow-waisted maiden. **(b)** Composite image of bilateral retrograde examinations performed in a patient with renal failure and minimal hydronephrosis shows narrowed areas in both ureters at the lumbosacral junction with medial deviation. This appearance has been described as the maiden waist deformity of the ureters. **(38)** Retroperitoneal fibrosis. **(a)** CT image of another patient demonstrates moderate hydronephrosis with delay in development of the tubular nephrogram on the right. **(b)** On CT scan obtained at a lower level, the right ureter can be seen entering a fibrotic plaque surrounding the aorta and inferior vena cava at the lumbosacral junction.

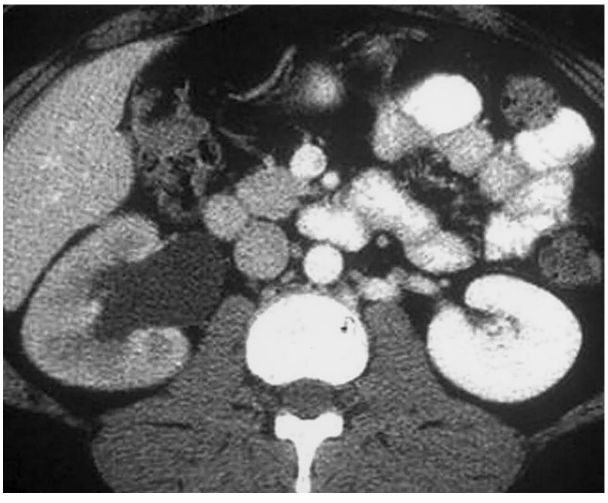

38a.

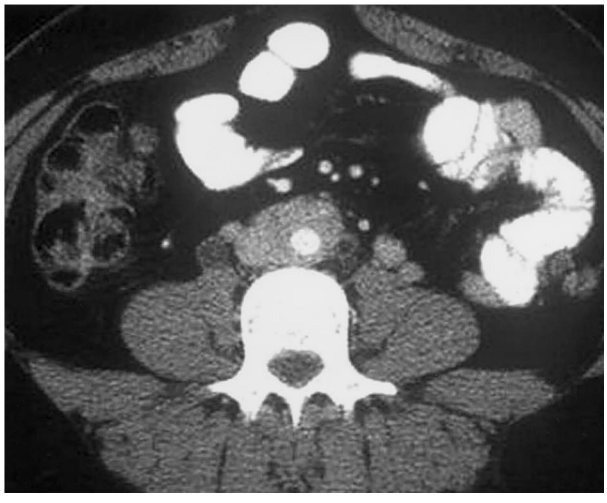

38b.

Maiden Waist Deformity (of Ureteral Deviation)

Retroperitoneal fibrosis is defined as the deposition of unencapsulated fibrous tissue, usually centered at the lumbosacral junction. The fibrotic plaque may encompass the ureters and may draw them medially, which results in alteration of the normal ureteral course and tapered narrowing of the opacified ureteral lumen. When the disease process involves both ureters, the ureteral course from the kidneys to the bladder is said to resemble a *narrow-waisted maiden* (Figs 37, 38) (39,40). Although idiopathic in up to 50% of cases (and called Ormond disease), retroperitoneal fibrosis can be associated with a variety of inflammatory insults including autoimmune disease or vasculitis, use of drugs such as methysergide and ergotamine, or traumatic retroperitoneal hemorrhage or urine leak; the condition may also develop as a response to tumor or in association with other fibrotic processes (40). Incongruity between the severe clinical degree of renal failure and the relatively mild degree of hydronephrosis seen at imaging may provide a diagnostic clue. Intraperitonealization (ie, surgical rerouting of ureters into the peritoneal cavity) of the ureters is

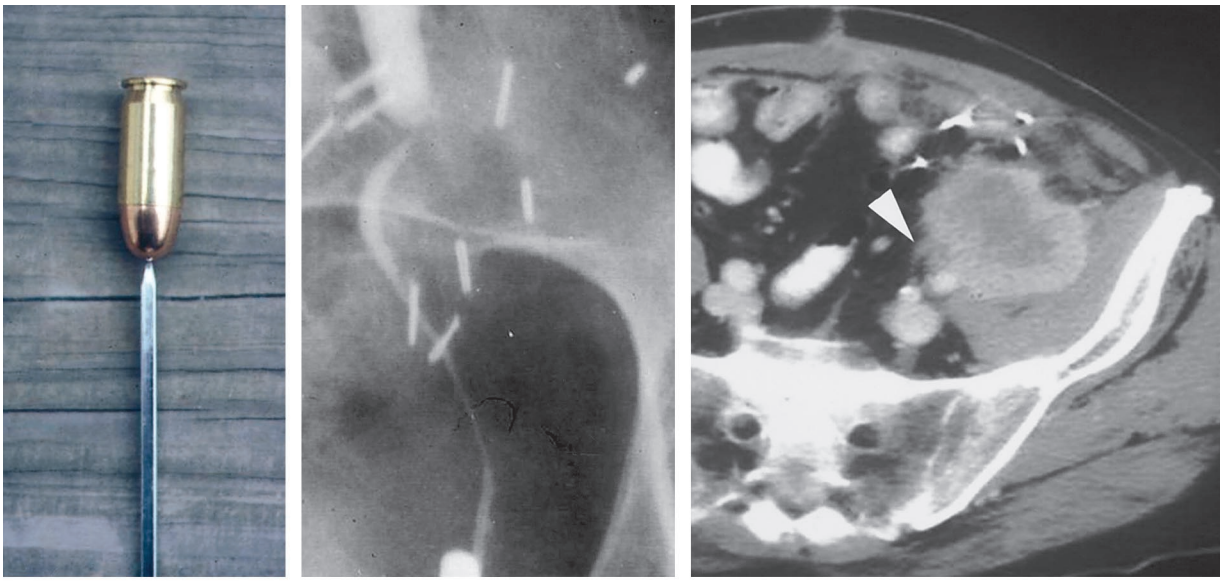

a. b. c.

Figure 40. **(a)** Bullet on a bodkin. **(b)** Retrograde ureteropyelogram demonstrates an abrupt transition between the dilated upper ureter and normal-appearing lower ureter. **(c)** Enhanced CT scan demonstrates encasement of the ureter (arrowhead) in the left anatomic pelvis by a mass, secondary to recurrent carcinoma of the colon.

Figure 39. Retroperitoneal fibrosis. Scout image of the abdomen shows bilateral stents in place in a patient who underwent intraperitonealization of the ureters as therapy for retroperitoneal fibrosis. Note the lateral position of the ureters associated with this intervention.

sometimes used as a therapeutic intervention to free the ureters from the fibrotic plaque and relieve associated obstruction. This intervention converts the ectomorphic position of the ureters into that of an endomorph (Fig 39).

Bullet and Bodkin Sign

Encasement of the ureter may produce an abrupt transition in ureteral caliber. The dilated ureter (the *bullet*) may appear to be precariously perched on the nondilated, encased ureter (the *bodkin*, which is defined as a sharp, slender instrument) (41). The bullet and bodkin appearance can be caused by metastatic disease, extension from an adjacent tumor (Fig 40), lymphoma, and rarely by benign inflammatory conditions such as retroperitoneal fibrosis.

Goblet Sign and Stipple Sign

The *goblet sign* describes the appearance of ureteral dilatation below the site of an intraluminal ureteral filling defect, best seen at retrograde ureteropyelography. The sign implies that the filling defect has been created by a chronic process, which has allowed the ureter below the site of the filling defect to accommodate to the lesion. The appearance is likely the result of mechanical dilatation of the ureter below the filling defect due to ureteral peristalsis (Fig 41) (42,43). Although originally described with transitional cell carcinoma of the ureter, the goblet sign may be seen

a. b.

Figure 41. **(a)** Goblet. **(b)** Retrograde ureteropyelogram, obtained to further evaluate a nonfunctional left kidney discovered at excretory urography, shows a filling defect due to transitional cell carcinoma, with dilatation of the ureter below the defect, producing the goblet sign.

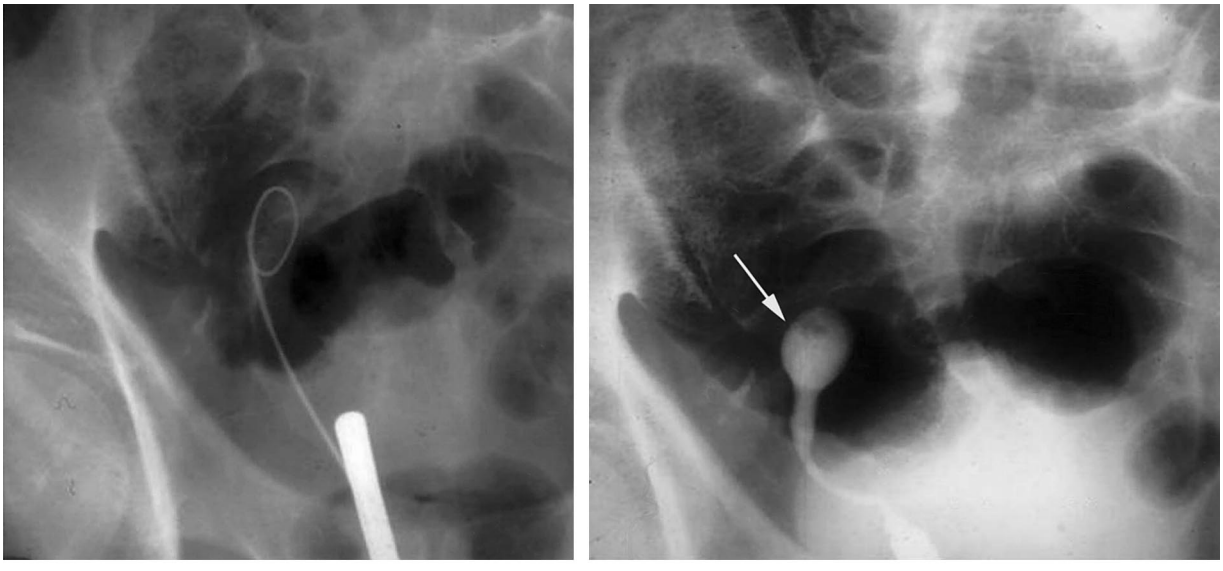

a. b.

Figure 42. Coiled catheter sign. **(a)** On a retrograde ureteropyelogram, persistent coiling of a guide wire was seen in the distal ureter during an attempt at retrograde stent placement. **(b)** Retrograde ureteropyelogram demonstrates dilatation of the ureter (arrow) below a site of complete ureteral obstruction caused by transitional cell carcinoma.

with any process, including metastatic disease or endometriosis, that slowly grows into the ureteral lumen. The dilated ureteral segment below the filling defect provides a potential space that may allow coiling of a catheter within it, if retrograde catheterization is attempted. The appearance of the catheter in this setting has been referred to as the *coiled catheter* sign (Fig 42) (42). At CT, the site of ureteral caliber transition should be closely

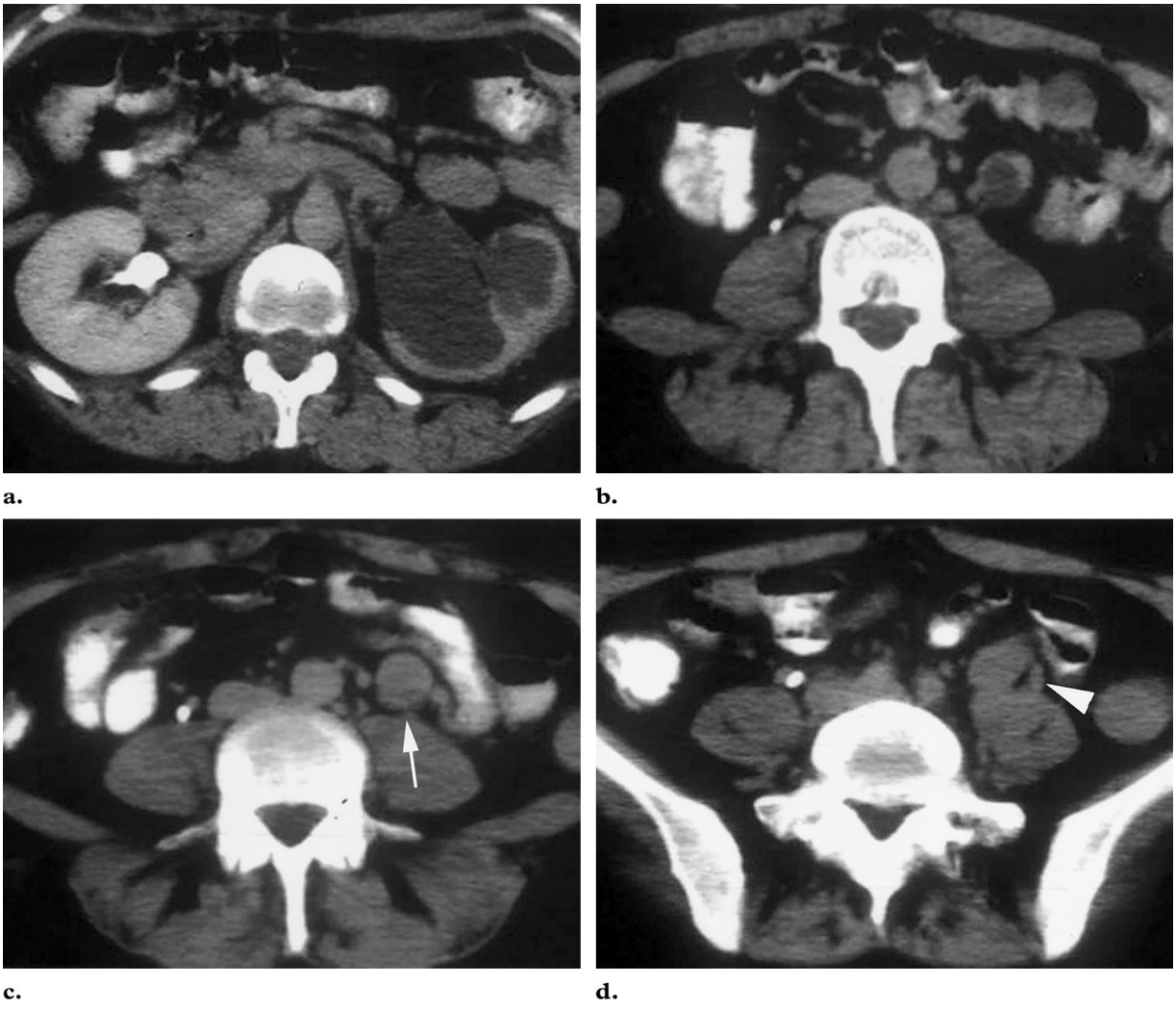

Figure 43. Ureteral transitional cell carcinoma. Sequence of enhanced CT scans, obtained after discovery of a nonfunctional left kidney, demonstrate hydronephrosis, hydroureter, and a soft-tissue mass in the distal left ureter (arrow in **c**). Note the transition to a normal ureter in **d** (arrowhead). These images provide an axial demonstration of the goblet sign.

inspected for the presence of an intraluminal soft-tissue mass, as a reflection of the goblet appearance (Fig 43) (43).

The artist Georges Seurat is known for his detailed pictures created with tiny dots of color, a style of painting called pointillism. Contrast material entrapped between the papillary projections of a transitional cell carcinoma can produce a pointillistic effect referred to as the *stipple sign* (44). This appearance is best seen in large papillary bladder tumors (Fig 44), but stippling may occur anywhere the papillary form of a urothelial tumor is fully expressed. Thus, it can be seen in other areas of the urinary tract and on any contrast-enhanced image.

Cobra Head Sign

Also known as the *spring onion* appearance, the *cobra head sign* refers to dilatation of the distal ureter, surrounded by a thin lucent line, which is seen in patients with adult-type (orthotopic) ureteroceles (Fig 45) (45,46). The distal ureter dilates in response to restriction of flow at the ureteral orifice in the bladder. The lucent hood represents the combined thickness of the ureteral wall and prolapsed bladder mucosa, outlined by contrast material within the bladder lumen. This lucent line should be thin and well defined. Any thickening, irregularity, or loss of definition of the

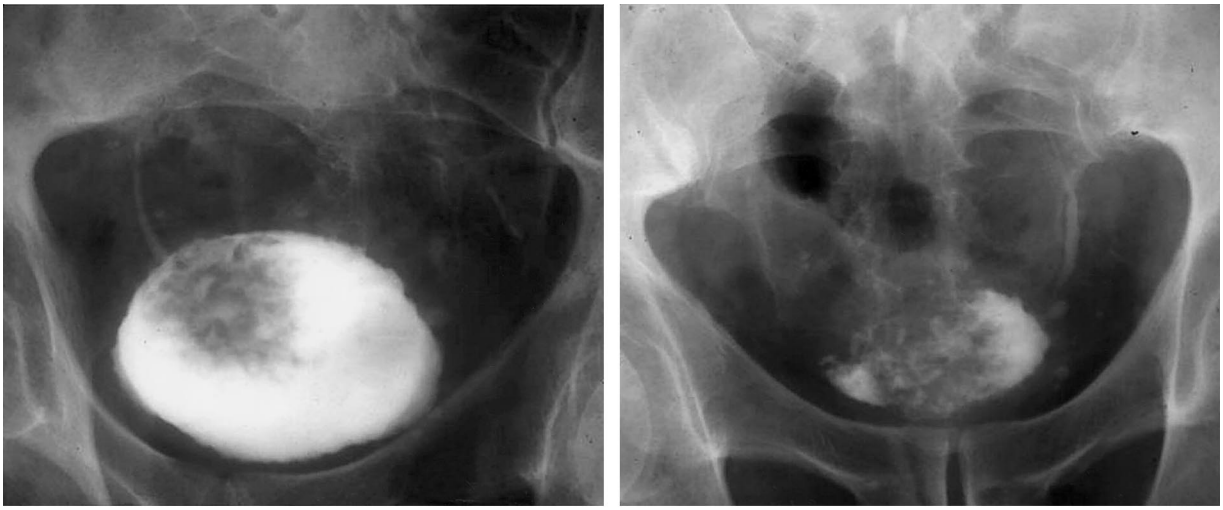

a. b.

Figure 44. Stipple sign. **(a)** Image from excretory urography shows a lesion with irregular margins that produces a filling defect in the upper aspect of the right side of the bladder. Note the dots of contrast material within the filling defect, the stipple sign. **(b)** Post-void image accentuates the findings. The appearance is typical of entrapment of contrast material between the projections of a papillary-type transitional cell carcinoma.

a. b.

Figure 45. **(a)** Cobra's head. **(b)** Late excretory urogram demonstrates bilateral ureteral obstruction from large, adult-type ureteroceles. Despite their size, the lucent rims surrounding the ureteroceles are thin and well defined.

cobra's hood should raise concern for the presence of a pseudoureterocele. A pseudoureterocele can result from edema related to stone impaction or recent stone passage, or more important, tumor overgrowth of the ureteral orifice (Figs 46, 47). If the appearance is not "classic," cystoscopic evaluation should be performed (45,46).

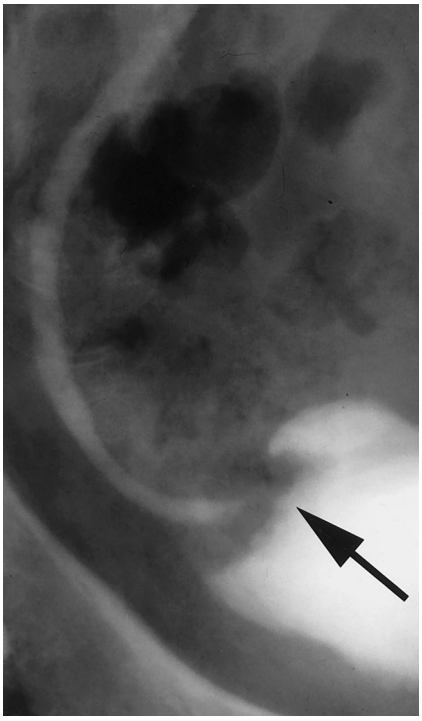

Figure 46. Pseudoureterocele. Excretory urogram shows a thickened, irregular halo (arrow) surrounding the distal ureter, caused by transitional cell carcinoma, resulting in a pseudoureterocele.

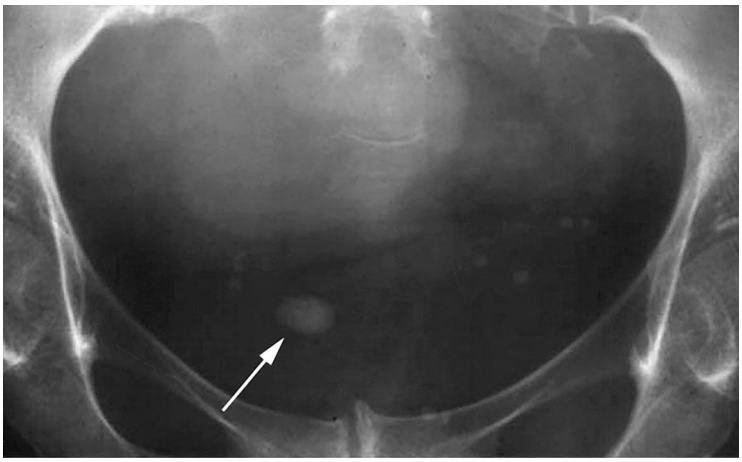

a.

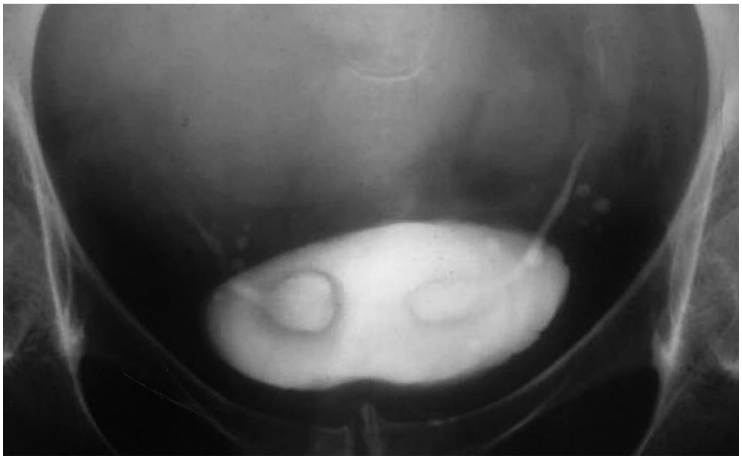

b.

Figure 47. Pseudoureterocele. **(a)** Excretory urogram obtained after lithotripsy shows stone fragments (arrow) that have impacted at the right ureterovesical junction. **(b)** Excretory urogram demonstrates dilatation of the distal ureter and a thickened, edematous halo surrounding the dilated segment. Prelithotripsy excretory urography had shown no such findings. Note the ureterocele on the left.

48a.

48b.

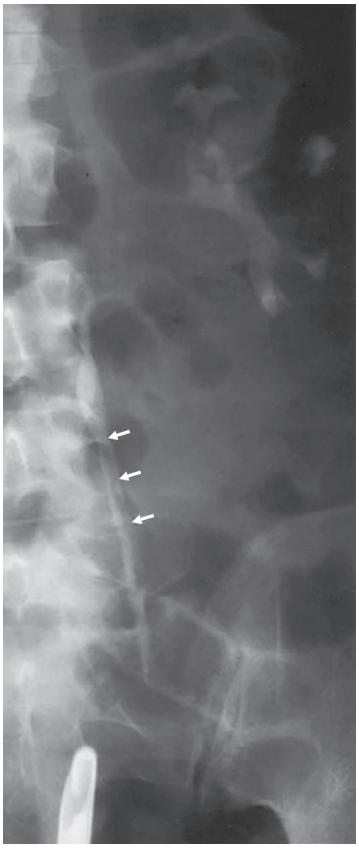

48c.

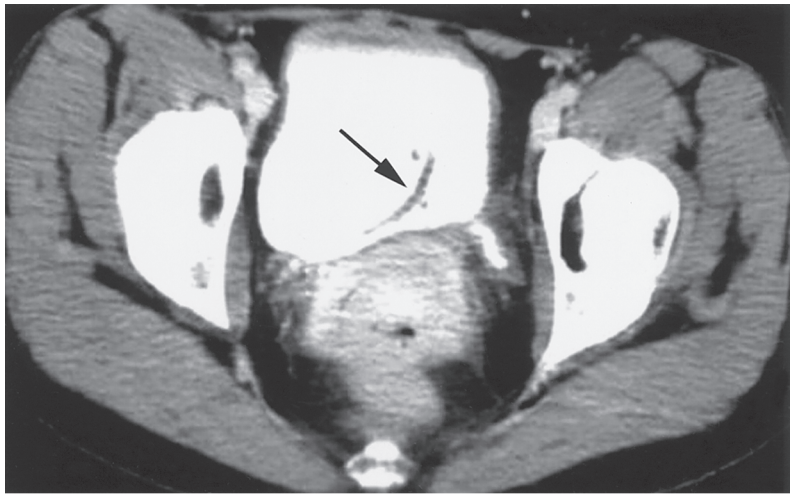

49.

Figures 48, 49. Spaghetti sign. **(48a)** Spaghetti. **(48b)** Excretory urogram shows an unusual filling defect in the right side of the bladder in a patient with gross hematuria. This defect resulted from a long clot being extruded into the bladder from the ureter. **(48c)** Retrograde ureteropyelogram demonstrates the linear clot in the left ureter (arrows), which was the result of an upper urinary tract transitional cell carcinoma. **(49)** CT scan demonstrates a linear filling defect (arrow), representing a clot extruded from the ureter, in the dependent portion of the bladder. Note the dilated left ureter, which was the source of the bleeding.

Spaghetti Sign

In a patient with gross hematuria, a linear filling defect within the bladder may result from extrusion of a blood clot from the ureter, which has acted as a mold. This *spaghetti sign* implies that the bleeding source is above the bladder, aiding the investigation of hematuria (Fig 48) (47). Although originally described at urography, the finding may occasionally be seen with other imaging modalities (Fig 49).

Pear-shaped and Pie-in-the-Sky Bladder

The normal round or oval shape of the opacified bladder may assume a *pear* or *tear drop* shape when it is symmetrically compressed in the

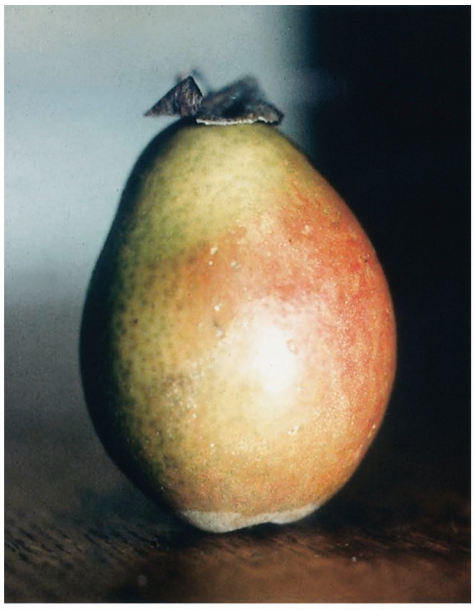

50a.

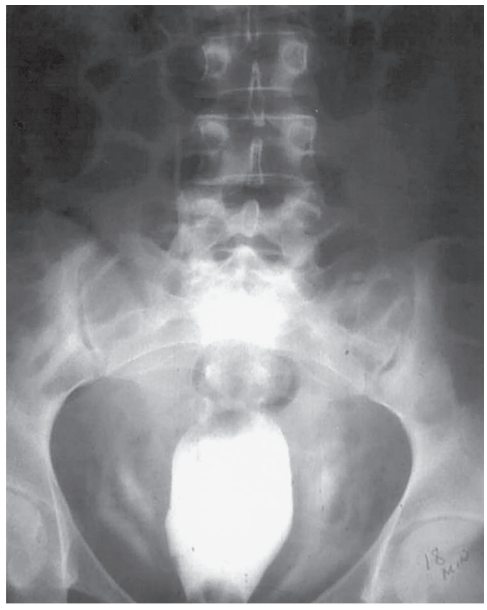

50b.

51a.

51b.

Figures 50, 51. **(50a)** Pear. **(50b)** Excretory urogram of a trauma victim. Pelvic trauma has resulted in extraperitoneal bladder rupture with urinary extravasation and pelvic hematoma, which produces symmetric compression of the bladder, resulting in the pear shape. **(51)** Pear-shaped bladder. **(51a)** Scout image shows perivesical lucency in a patient with pelvic lipomatosis. **(51b)** Excretory urogram demonstrates medial deviation of the distal ureters, which is an associated finding in pelvic lipomatosis. Note the compression of the bladder, giving it a pear shape.

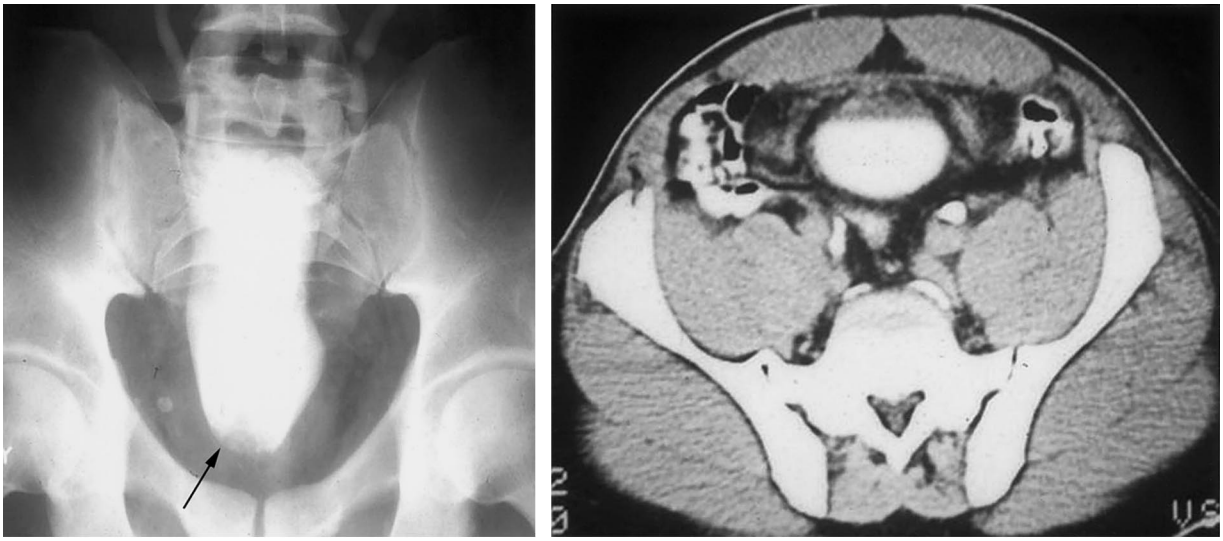

a. **b.**

Figure 52. Pear-shaped bladder. **(a)** Excretory urogram demonstrates filling defects (arrow) in the bladder base, which proved to be cystitis glandularis, associated with symmetric bladder compression. **(b)** Although cystitis glandularis has been associated with pelvic lipomatosis, in this case, the CT scan reveals the compression is caused by psoas muscle hypertrophy.

Figure 53. Pie-in-the-sky bladder. Scout image of the pelvis, obtained after administration of contrast material for CT, demonstrates bilateral pubic rami fractures. The associated pelvic hematoma elevates the bladder, giving it the pie-in-the-sky appearance. There was an associated posterior urethral injury.

anatomic pelvis by an extrinsic process (Fig 50). The differential diagnosis of the imaging appearance includes the presence of pelvic fluid (hematoma, lymphocele, urinoma, or abscess), pelvic lipomatosis (Fig 51), vascular dilatation (aneurysm or collateral vessel development), symmetric lymph node enlargement, or psoas muscle hypertrophy. CT is the most helpful examination for determining the specific cause of the finding (Fig 52) (47–49).

A *pie-in-the-sky bladder* may also be seen with pelvic trauma. The sign refers to a high position of the opacified bladder within the pelvis at imaging and implies the presence of a large pelvic hematoma, associated with disruption of the bladder moorings. Observation of this sign should raise concern for an associated urethral injury (Fig 53) (50).

a.

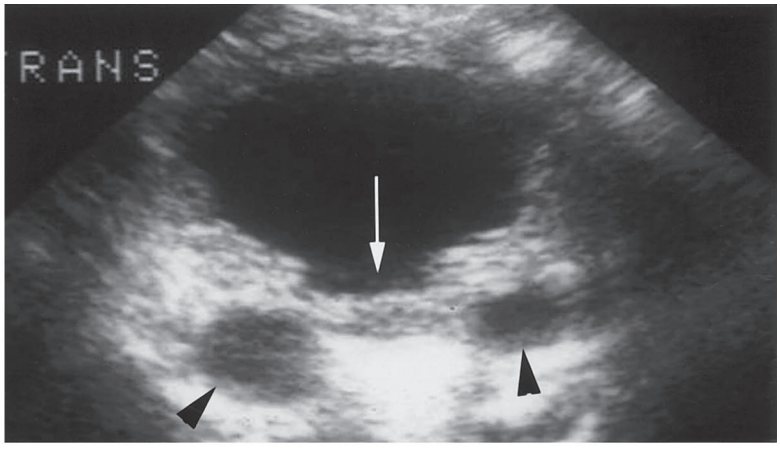

b.

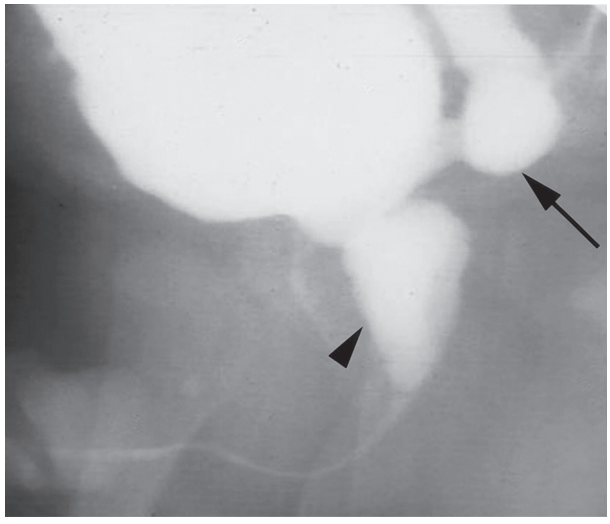

c.

Figure 54. **(a)** Keyhole. **(b)** Transverse US image of the bladder in a male infant demonstrates bladder wall thickening and dilatation of the posterior urethra, resulting in a keyhole appearance (arrow). Note the dilated ureters posterior to the bladder (arrowheads). **(c)** Image from voiding cystourethrography in the same patient demonstrates dilatation of the urethra proximal to posterior urethral valves (arrowhead), with reflux into the dilated distal ureter (arrow).

Keyhole Sign

Sonographic identification of hydronephrosis in a male fetus or infant should prompt investigation for the presence of posterior urethral valves. The thick-walled bladder and dilated posterior urethra related to obstruction by the valves, as seen at US, may resemble a *keyhole* (51). The more familiar appearance of posterior urethral valves seen at voiding cystourethrography reinforces the sonographic findings (Fig 54).

Threads and Streaks Sign

The *threads and streaks sign* was originally a description of the angiographic appearance of vascularized tumor thrombus extending into the renal vein or inferior vena cava from a renal cell carcinoma. Recognition of the sign is important, because it may mean that the surgical approach to the renal tumor must be altered. At angiography, opacified vessels supplying the intravascular tumor may produce a linear, threadlike, or stringlike appearance (Fig 55) (52). Cross-sectional images and multiplanar reconstructions from CT or MR imaging studies may also reveal the sign (Fig 56).

Spoked Wheel Pattern

The *spoked wheel* description was applied to the angiographic appearance of the vascular pattern seen in some oncocytomas. Centripetal "spoke" vessels arising from a peripheral "rim" vessel were initially thought to be characteristic of this tumor (Fig 57). However, the pattern is now known to be nonspecific, and a similar vascular arrangement has been described with renal cell carcinoma (53). The angiographic appearance may relate to the presence of a pseudocapsule and a stellate, central scar, which can be seen in some oncocytomas larger than 3 cm in diameter (54). The scar has been described at US, CT (Fig 58), and MR imaging.

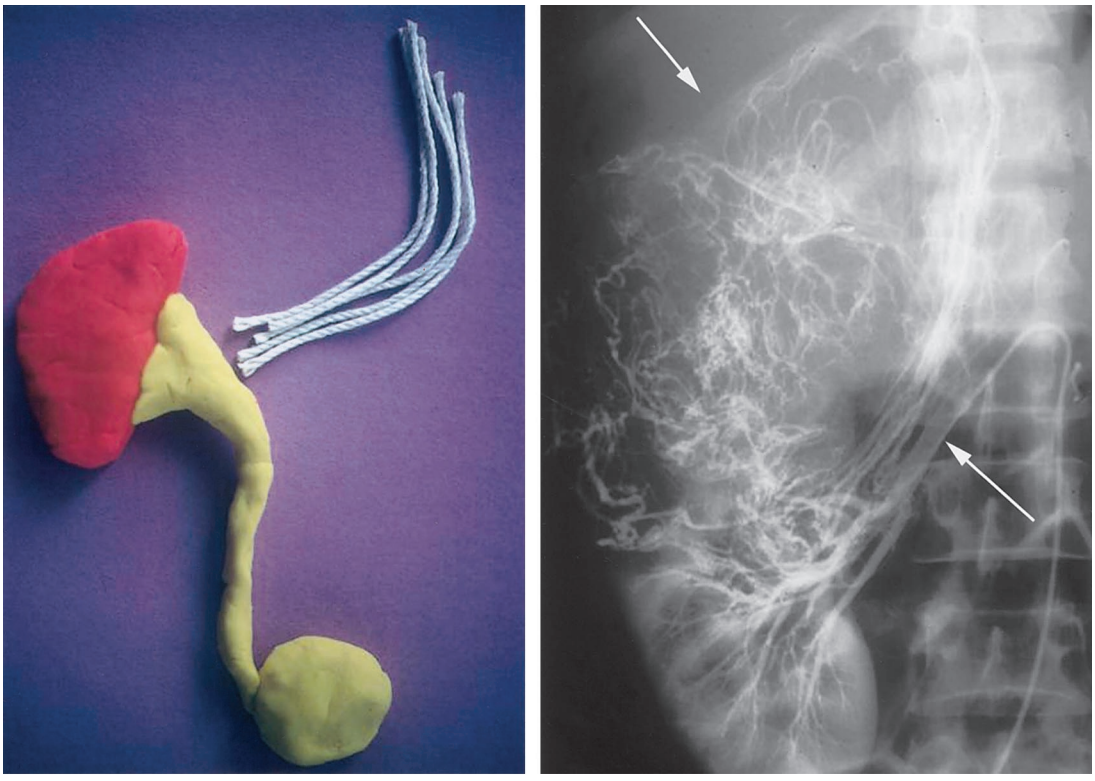

a. b.

Figure 55. **(a)** Threads and streaks. **(b)** Late phase image from selective right renal arteriography demonstrates distortion of the normal vascular arborization pattern in the upper portion of the right kidney (upper arrow) with linear vessels (lower arrow) extending into vascularized tumor thrombus in the right renal vein and inferior vena cava.

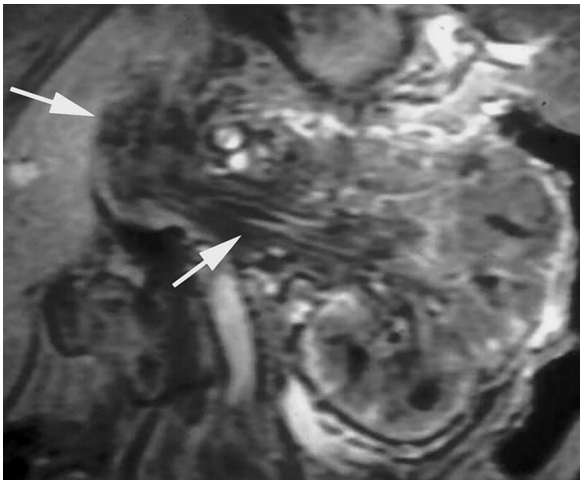

Figure 56. Threads and streaks. Gadolinium-enhanced, coronal T1-weighted MR image of the left kidney in another patient with a left upper pole renal mass shows linear vascularity supplying a tumor thrombus extending along the left renal vein and into the inferior vena cava (arrows).

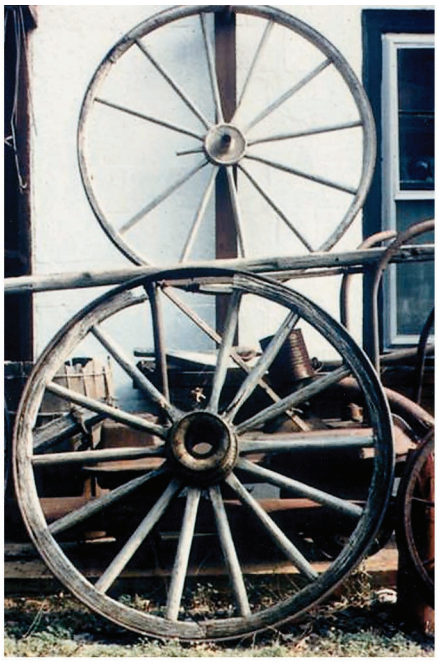

57a.

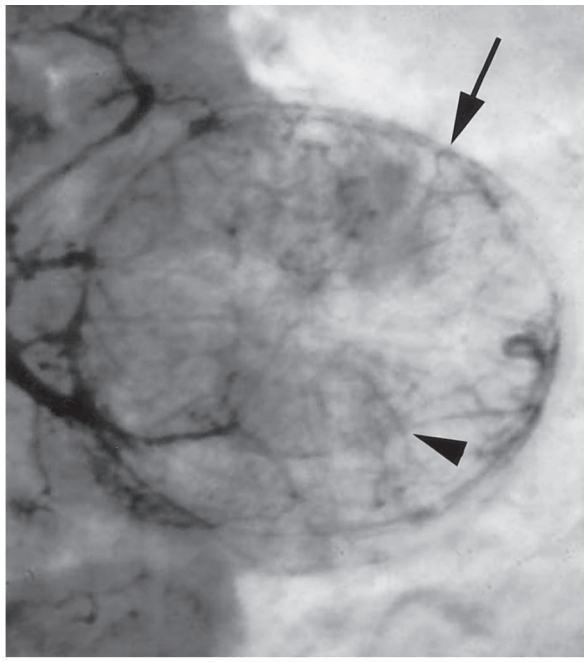

57b.

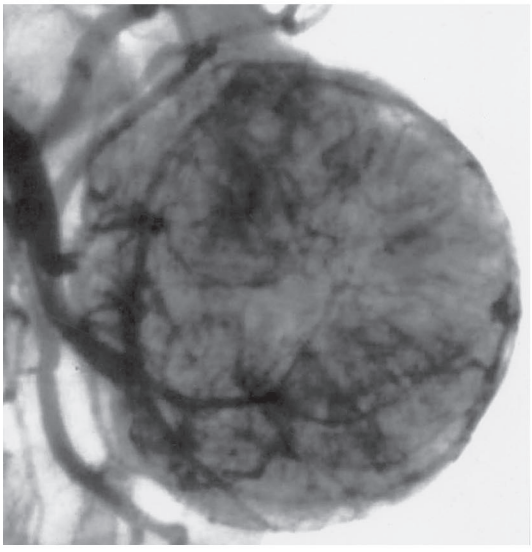

57c.

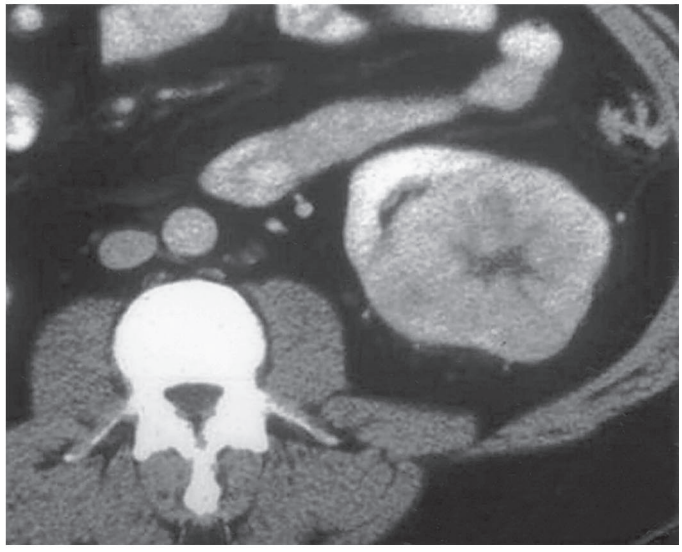

58.

Figures 57, 58. Spoked wheel pattern. **(57a)** Spoked wheels. **(57b)** Collimated view from selective left renal arteriography shows a mass in the interpolar region of the kidney with a peripheral rimming vessel (arrow) and centripetal vessels projecting into the mass (arrowhead), resembling the rim and spokes of a wagon wheel. **(57c)** Late phase image shows decreased vascularity in the central portion of the mass consistent with a scar. The mass was a surgically proved oncocytoma. **(58)** Renal oncocytoma. Enhanced CT image shows a left renal mass with a relatively homogeneous enhancement pattern, except for a stellate central scar. Although the pattern may be seen with an oncocytoma, as in this case, it has also been described with renal cell carcinoma.

String of Pearls Appearance

The descriptive term *string of pearls* has been applied to the angiographic appearance of arteries involved with the medial form of fibromuscular dysplasia (55). Thickened fibromuscular ridges, alternating with areas of wall thinning and aneurysm formation, create the typical appearance, most often seen in the renal arteries (Fig 59) (55,56). The presence of fibromuscular dysplasia as a cause of renovascular hypertension is always a consideration in children and middle-aged women. Distinction of fibromuscular dysplasia from atherosclerotic disease is important for proper therapeutic intervention. Improving resolution of CT angiography and MR angiography should allow identification of the sign with these techniques as well (Fig 60).

59a.

60.

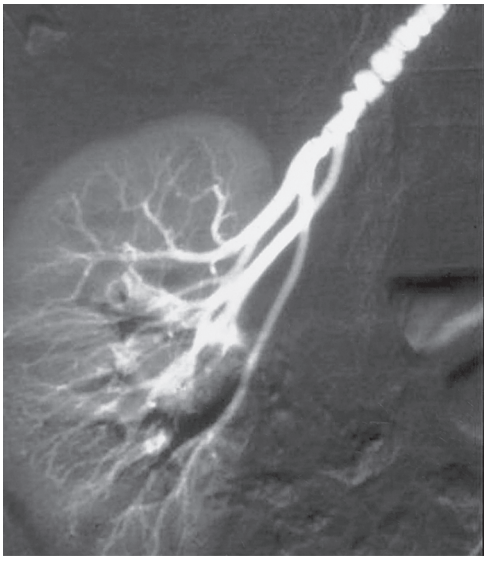

59b.

Figures 59, 60. String of pearls appearance. **(59a)** String of pearls. **(59b)** Selective right renal arteriogram shows areas of aneurysmal dilatation alternating with areas of stenosis in the distal main renal artery, giving the typical string of pearls appearance associated with the medial form of fibromuscular dysplasia. **(60)** Gadolinium-enhanced MR angiographic image of another patient with fibromuscular dysplasia also demonstrates the string of pearls appearance in the right renal artery. (Case courtesy Peter L. Choyke, MD, National Institutes of Health, Bethesda, Md.)

Conclusions

The familiarity afforded by recognition of a classic sign or Aunt Minnie allows for a more confident diagnosis. Newer imaging modalities may render some signs obsolete, but they do not change the basic pathophysiology on which the signs are based; rather, we must reinterpret these "old stand-bys." Newer imaging modalities beget new signs each day. At the end of the day, perhaps a familiar face will make the interpretive process a bit easier and a bit more fun.

Acknowledgments: The authors thank Christopher Dyer, Richard Dyer, and Susanna Dyer for their assistance with creation of several illustrations.

References

1. Dyer RB, Chen MY, Zagoria RJ. Abnormal calcifications in the urinary tract. RadioGraphics 1998; 18:1405–1424.
2. Penter G, Arkell DG. The fragmented staghorn calculus: a radiological sign of pyonephrosis. Clin Radiol 1989; 40:61–63.
3. Parker MD, Clark RL. Evolving concepts in the diagnosis of xanthogranulomatous pyelonephritis. Urol Radiol 1989; 11:7–15.
4. Lloyd-Thomas HG, Balme RH, Key JJ. Tram-line calcification in renal cortical necrosis. BMJ 1962; 5282:909–911.
5. Palubinskas AJ. Renal pyramidal structure opacification in excretory urography and its relation to medullary sponge kidney. Radiology 1963; 81:963–970.
6. Lalli AF. Renal parenchymal calcifications. Semin Roentgenol 1982; 17:101–112.
7. Winfield AC, Gerlock AJ Jr, Shaff MI. Perirenal cobwebs: a CT sign of renal vein thrombosis. J Comput Assist Tomogr 1981; 5:705–708.
8. Feuerstein IM, Zeman RK, Jaffe MH, Clark LR, David CL. Perirenal cobwebs: the expanding CT differential diagnosis. J Comput Assist Tomogr 1984; 8:1128–1130.
9. Kunin M. Bridging septa of the perinephric space: anatomic, pathologic, and diagnostic considerations. Radiology 1986; 158:361–365.
10. Smith RC, Dalrymple NC, Neitlich J. Noncontrast helical CT in the evaluation of acute flank pain. Abdom Imaging 1998; 23:10–16.
11. Heneghan JP, Dalrymple NC, Verga M, Rosenfield AT, Smith RC. Soft-tissue "rim" sign in the diagnosis of

ureteral calculi with use of unenhanced helical CT. Radiology 1997; 202:709–711.
12. Bell TV, Fenlon HM, Davison BD, Ahari HK, Hussain S. Unenhanced helical CT criteria to differentiate distal ureteral calculi from pelvic phleboliths. Radiology 1998; 207:363–367.
13. Hann L, Pfister RC. Renal subcapsular rim sign: new etiologies and pathogenesis. AJR Am J Roentgenol 1982; 138:51–54.
14. Kamel IR, Berkowitz JF. Assessment of cortical rim sign in posttraumatic renal infarction. J Comput Assist Tomogr 1996; 20:803–806.
15. Jordan J, Low R, Jeffrey RB Jr. CT findings in acute renal cortical necrosis. J Comput Assist Tomogr 1990; 14: 155–156.
16. Agarwal A, Sakhuja V, Malik N, Chugh KS. Diagnostic value of CT scan in acute renal cortical necrosis. Renal Failure 1992; 14:193–196.
17. Elkin M. Obstructive uropathy and uremia. Radiol Clin North Am 1972; 10:447–465.
18. Winograd J, Schimmel DH, Palubinskas AJ. The spotted nephrogram of renal scleroderma. Am J Roentgenol 1976; 126:734–738.
19. Pope TL Jr, Buschi AJ, Moore TS, Williamson BR, Brenbridge AN. CT features of renal polyarteritis nodosa. AJR Am J Roentgenol 1981; 136:986–987.
20. Dunbar JS, Nogrady MB. The calyceal crescent—a roentgenographic sign of obstructive hydronephrosis. Am J Roentgenol Radium Ther Nucl Med 1970; 110: 520–528.
21. Levine M, Allen A, Stein JL, Schwartz S. The crescent sign. Radiology 1963; 81:971–973.
22. Bush WH, Branner GE, Lewis GP. Ureteropelvic junction obstruction treatment with percutaneous endopyelotomy. Radiology 1989; 171:535–538.
23. Hahn PF, Saini S, Stark DD, Papanicolaou N, Ferrucci JT Jr. Intraabdominal hematoma: the concentric-ring sign in MRI. AJR Am J Roentgenol 1987; 148:115–119.
24. Yassa NA, Peng M, Ralls PW. Perirenal lucency ("kidney sweat"): a new sign of renal failure. AJR Am J Roentgenol 1999; 173:1075–1077.
25. Nino-Murcia M, deVries PA, Friedland GW. Congenital anomalies of the kidney. In: Pollack HM, McClennan BL, eds. Clinical urography. 2nd ed. Philadelphia, Pa: Saunders, 2000; 690–763.
26. Mascatello V, Lebowtiz RL. Malposition of the colon in left renal agenesis and ectopia. Radiology 1976; 120: 371–376.
27. Hoffman CK, Filly RA, Callen PW. The "lying down" adrenal sign: a sonographic indicator of renal agenesis or ectopia in fetuses and neonates. J Ultrasound Med 1992; 11:533–536.
28. Felson B, Moskowitz M. Renal pseudotumors: the regenerated nodule and other lumps, bumps and dromedary humps. Am J Roentgenol Radium Ther Nucl Med 1969; 107:720–729.
29. Thornbury JR, McCormick TL, Silver TM. Anatomic/radiologic classification of renal cortical nodules. AJR Am J Roentgenol 1980; 134:1–7.
30. Hodson CJ, Mariani S. Large cloisons. AJR Am J Roentgenol 1982; 139:327–332.
31. Kollins SA, Hartman GW, Carr DT, Segura JW, Hattery RR. Roentgenographic findings in urinary tract tuberculosis: a 10 year review. Am J Roentgenol Radium Ther Nucl Med 1974; 121:487–499.
32. Becker JA. Renal tuberculosis. Urol Radiol 1988; 10:25–30.
33. Dunnick NR, Sandler CM, Newhouse JH, Amis ES Jr. Textbook of uroradiology. 3rd ed. Baltimore, Md: Williams & Wilkins, 2001; 300.
34. Hartman GW, Torres VE, Leago GF, Williamson B, Hattery RR. Analgesic-associated nephropathy. JAMA 1984; 251:1734–1738.
35. Brennan RE, Pollack HM. Nonvisualized ("phantom") renal calyx: causes and radiologic approach to diagnosis. Urol Radiol 1979; 1:17–23.
36. Hulnick DH, Bosniak MA. "Faceless kidney": CT sign of renal duplicity. J Comput Assist Tomogr 1986; 10: 771–772.
37. Fernbach SK, Feinstein KA, Spencer K, Lindstrom CA. Ureteral duplication and its complications. RadioGraphics 1997; 17:109–127.
38. Callahan MJ. The drooping lily sign. Radiology 2001; 219:226–228.
39. Arger PH, Stolz JL, Miller WT. Retroperitoneal fibrosis: an analysis of the clinical spectrum and roentgenographic signs. Am J Roentgenol Radium Ther Nucl Med 1973; 119:812–821.
40. Amis ES Jr. Retroperitoneal fibrosis. AJR Am J Roentgenol 1991; 157:321–329.
41. Kunin M, Goodwin WE. The encased ureter: bullet and bodkin pattern, a reliable radiographic sign. Br J Urol 1990; 66:471–474.
42. Bergman H, Friedenberg RM, Sayegh V. New roentgenologic signs of carcinoma of the ureter. Am J Roentgenol Radium Ther Nucl Med 1961; 86:707–717.
43. Ramchandani P, Pollack HM. Tumors of the urothelium. Semin Roentgenol 1995; 30:149–167.
44. McLean GK, Pollack HM, Banner MP. The "stipple" sign—urographic harbinger of transitional cell neoplasms. Urol Radiol 1979; 1:77–79.
45. Mitty HA, Schapira HE. Ureterocele and pseudoureterocele: cobra versus cancer. J Urol 1977; 117:557–561.
46. Thornbury JR, Silver TM, Vinson RK. Ureteroceles vs. pseudoureteroceles in adults. Radiology 1977; 122:81–84.
47. Komolafe F. The "spaghetti sign": an uncommon radiologic sign of upper urinary tract hemorrhage. AJR Am J Roentgenol 1981; 137:1062.
48. Ambos MA, Bosniak MA, Lefleur RS, Madayag MA. The pear-shaped bladder. Radiology 1977; 122:85–88.
49. Wechsler RJ, Brennan MD. Teardrop bladder: additional considerations. Radiology 1982; 144:281–284.
50. Sandler CM, McCallum RW. Urethral trauma. In: Pollack HM, McClennan BL, eds. Clinical urography. Philadelphia, Pa: Saunders, 2000; 1819–1837.
51. Callen PW. Ultrasound in obstetrics and gynecology. 3rd ed. Philadelphia, Pa: Saunders, 1994; 400.
52. Ferris EJ, Bosniak MA, O'Connor JF. An angiographic sign demonstrating extension of renal carcinoma into the renal vein and vena cava. Am J Roentgenol Radium Ther Nucl Med 1968; 102:384–391.
53. Older RA, Cleeve DM, Fetter BF, Jackson DA. "Spokewheel" angiographic pattern in renal masses: nonspecificity (letter). Radiology 1978; 128:836.
54. Newhouse JH, Wagner BJ. Renal oncocytomas. Abdom Imaging 1998; 23:249–255.
55. Lassiter FD. The string-of-beads sign. Radiology 1998; 206:437–438.
56. McCormack LJ, Dustan HP, Meaney TF. Selected pathology of the renal artery. Semin Roentgenol 1967; 2:126–138.

This article meets the criteria for 1.0 credit hour in category 1 of the AMA Physician's Recognition Award. To obtain credit, see accompanying test at http://www.rsna.org/education/rg_cme.html.